14

Testing Methods in Filled Systems

This chapter contains a discussion of the following subjects related to the analysis of filled systems:

- The reasons for the use of a particular testing method
- The procedures used for testing
- Available standard methods
- Major findings by various analytical techniques.

The testing methods are divided into two groups: physical methods and chemical and instrumental analysis. Within the group, the testing methods are discussed in alphabetic order according to the same pattern.

14.1 PHYSICAL METHODS

14.1.1 ATOMIC FORCE MICROSCOPY[1-3]

Applications: Atomic force microscopy is an efficient tool for the analysis of surface topography and also surface mechanical properties such as friction and elasticity. It can be used to reveal molecular or atomic order with spatial resolution higher than that of electron microscopy. Hard and flat surfaces can be observed without difficulties. Soft and rough samples may produce image artifacts. The following uses are known in filled systems: determination of surface morphology and nanostructure of high modulus polyethylene fibers,[1] structure and morphology of small diameter (13 μm) aramid fibers,[2] and carbon black aggregates.[3]

Testing procedure: Probing repulsive force variations between a very small probe (usually apex radius smaller than 10 nm) and a sample, one can observe surface morphology. Nanoscope from Digital Instruments, Inc., Santa Barbara, California is an instrument chosen in reported applications. The microscope stage allows for sample rotation. Several different probes are used (probes for high magnification of atomic order differ from the probes for macroscopic examinations). Also, different software is available. Samples can be observed in air, but spatial resolution can be enhanced and surface damage avoided by observing samples under water. Surface damage can also be limited by scanning in constant force mode. Sample preparation is very important. A microscope cover slip glass is a frequent substrate used. This glass is cut to smaller sections, for example, 3×3 mm. The sample is deposited

on the wet glass piece and dried under vacuum at room temperature.[2] A more complex procedure was used in preparation of carbon black aggregates for observation.[3] Carbon black (20 mg) was ultrasonically dispersed in chloroform (40 ml), then a few microliters deposited on glass pieces. In order to obtain a uniform distribution and density of aggregates, the suspension was also deposited by two or three consecutive deposits in the same location. It was also noticed that the surface of the glass support has an important effect on uniformity of distribution. A gold-coated surface gave a more uniform distribution than straight glass and was the substrate of choice for carbon black samples.[3]

Standard methods: none

Major results: The smallest nanofibrils detected had a width of 10-15 nm (even smaller fibers of 5-8 nm can be seen).[1] The vertical resolution of atomic force microscopy is superior to scanning electron microscopy; therefore, peculiarities of fiber morphology can be easily observed. The results of fiber diameter measurement are in agreement with X-ray diffraction experiments. Roughness parameters of aramid fibers can be determined, which help in improving process conditions.[2] Carbon black aggregates had heights of 50 to 150 nm, which are higher than detected by TEM (20 nm).[3] It is postulated that the understanding of structure of carbon black should be reviewed after broader data on carbon black become available.[3] It is possible that the present understanding is based on artifacts related to the previously used methods such as SEM and TEM.

14.1.2 AUTOIGNITION TEST[4]

Applications: Determination of specimen autoignition.

Testing procedure: Temperature of specimen is kept constant at 430°C in the presence of air, and time to autoignition is measured. In another version, the oxygen atmosphere is modified, and the temperature of autoignition is recorded.

Standard methods: ASTM D 1929

Major results: Figure 12.3 shows that talc and $Mg(OH)_2$ increase ignition time with increasing concentration of filler.

14.1.3 BOUND RUBBER[5]

Applications: Bound rubber is a measure of filler surface activity to the matrix, and it is considered as a factor in the estimation of filler reinforcement.

Testing procedure: Small pieces of uncured rubber are immersed for several days at room temperature in a large excess of good solvent such as toluene. The sample in contact with solvent becomes divided into three parts: polymer solution, m_{pI}, solvent-dispersed filler particles with absorbed polymer chains, m_{pII}, and solvent-swollen gel of filler particles connected through polymer chains, m_{pIII}. The fraction of polymer bound to filler is determined from the equation: $B = \left(m_{pII} + m_{pIII}\right) / m_p$ where m_p is total mass of polymer. The fraction of polymer not dispersed by solvent is given by the following equation: $G = m_{pIII} / m_p$.

Standard methods: NF T 45-114

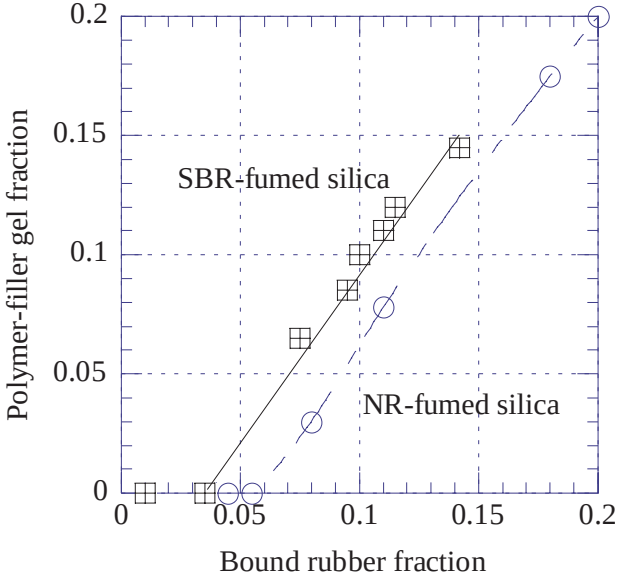

Figure 14.1. Polymer-filler gel vs. bound rubber fraction. [Adapted, by permission, from Karasek L, Sumita M, *J. Mat. Sci.*, **31**, No.2, 1996, 281-9.]

Major results: Figure 14.1 shows that at smaller concentrations of filler, there is only absorption of polymer on solvent-dispersed filler. When concentration increases, the gel is formed. Higher molecular weight polymer is bound preferentially. There are many factors influencing bound rubber measurement.[5] With regard to filler, these include concentration, size of aggregates, surface area, and surface activity (functional groups, free radicals from aggregate breakdown, graphitization, coupling agents, hydrophobic agents, surface active agents). Elastomer affects bound rubber determination depending on chemical composition, unsaturations, stability (thermal, mechano-chemical, and oxidative). Several additives affect the determination of bound rubber. These include free radical terminators, promoters, coupling agents, and surface active agents. Other parameters include mixing variables and temperature of extraction. With this variability, results are frequently questionable.

14.1.4 CHAR FORMATION[6]

Applications: The method is used to determine the effect of formulation variables on char formation and the stability of char to further pyrolysis.

Testing procedure: A tube furnace is 1 m long and has a 7.2 cm diameter. At one end of the tube, a forced air flow is supplied. The furnace temperature is measured by a thermocouple located 30 cm from the end of air supply. The temperature is constant within ±2°C and is kept at 600°C. The sample is placed in a holder made from a ceramic material with a tungsten foil lining. In the oxygen-free mode, no air flows in the furnace, but a dry air is supplied at the rate of 1 m^3/min in the oxygen-

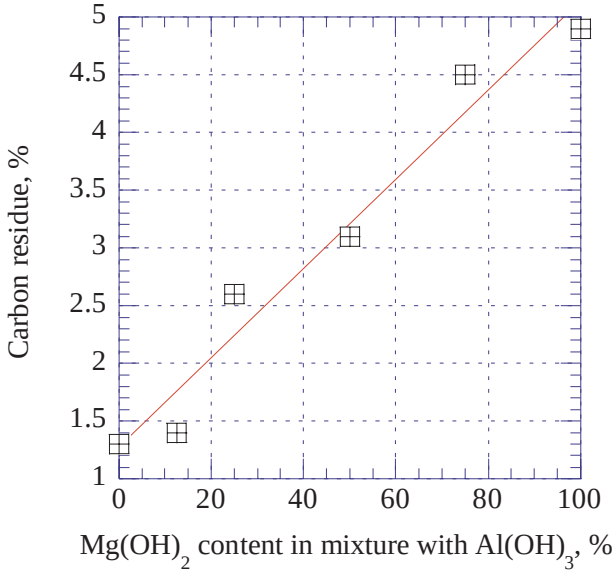

Figure 14.2. Carbon residue remaining from the decomposition of EPDM at 600°C for 5 min vs. percentage of $Mg(OH)_2$ in the mixture with $Al(OH)_3$. [Data from Levesque J L, Fraval J T, Antec '93. Conference Proceedings, New Orleans, La., 9th-13th May 1993, Vol. II, 1957-64.]

ated mode. Typically, the oxygen-free mode was used because of better repeatability.[6] The samples ($1 \times 4 \times 0.2$ cm) are placed on wire grid, left in the oven for a specific period of time, removed, immersed in liquid nitrogen to stop the combustion process, and carbon residue determined.

Standard methods: AS 2122

Major results: Figure 14.2 shows the results of determination of char formation in EPDM filled with a mixture of $Al(OH)_3$ and $Mg(OH)_2$. $Mg(OH)_2$ is more efficient in char formation.

14.1.5 CONE CALORIMETRY[4,7-11]

Applications: A cone calorimeter, named after a truncated cone shape of the furnace, is a heat release rate calorimeter which permits the determination of heat release under controlled conditions. It determines the critical fire parameters required for a range of natural and synthetic materials using small samples (100 mm^2), and simple materials, and is used for composites and combinations of different materials. This apparatus allows simultaneous and continuous determinations of heat release rate, smoke production rate, mass loss rate, concentration of the various combustion gases formed, ignitability, heat of combustion and soot production data for the materials tested.

Testing procedure: The equipment was developed by NIST and is produced by PL Thermal Sciences, 300 Washington Blvd., Mundelein, IL 60060, USA. Testing according to ISO 5660 requires a heat flux of 25 kW/m^2 and an air flow 24 l/s. The

heat released is calculated based on oxygen depletion due to combustion. The mass of the specimen, the rate of mass loss, the time to ignition, the rate of heat release and its maximum value are calculated for the first 3 min of burning by a supplied software. The instrument also calculates specific extinction area, which is the increase of extinction area of the smoke divided by the unit mass of material decomposing to volatile products.

Standard methods: ASTM E 1740, BS 476:Part 1, ISO 5660

Major results: Due to the computerized determination of many parameters of material combustion and the well controlled process of combustion, this instrument is frequently used in studies of materials containing fillers.

14.1.6 CONTACT ANGLE[12-25]

Applications: The following uses of contact angle were reported in the literature: surface energy of different sizes for fibers,[12] correlation between contact angle of fiber and interlaminar shear strength of composite,[12] effect of surface treatment of fillers for paints,[13] the matrix-filler adhesion parameter for PS filled with $CaCO_3$,[14] dispersion stability of PEO-modified kaolin particles,[16] determination of contact angle of carbon fibers and its dependence on treatment,[17] wettability of fiber surfaces,[20] effect of fillers on surface free energy of paper coatings,[16] cleanliness of fibers,[22] wetting of filler by polymer,[23] and adhesion between layers.[25]

Testing procedure: Several methods are used to determine contact angle. The method of choice depends on the sample type. The most common method used for larger, flat samples is a goniometer method. A water droplet is placed on the material surface and contact angle determined either by optical methods (older instruments) or by the use of software which analyzes the image and calculates the contact angle. The precision of determination depends on sample preparation and time of measurement. Samples with surface roughness and imperfections give confusing results. Also, materials which are rapidly wetted by the liquid used give results of very low precision. The availability of a great number of instruments of different levels of computerization makes a precise determination of contact angle possible. Particulate fillers and fibers are difficult to measure because of their small dimensions. In the case of fibers, the tensiometer method gives precise measurements.[12] One end of the fiber is hung vertically from the arm of an electromicrobalance, and the other end is immersed into the liquid. From the Fowkes equation, interfacial free energies can be calculated. Goniometer was also successfully used to determine the contact angle of the fiber.[12] A precise method was developed based on photographic images taken under the microscope.[17] The method eliminates errors due to the influence of surface roughness of fiber. In the case of particulate fillers, three options are available: determination of the surface energy by inverse gas chromatography,[18,19] the captive droplet technique,[16] and the filler column method.[14] Inverse gas chromatography is discussed in a separate section below. In the captive droplet technique, a smooth surface is obtained by press-

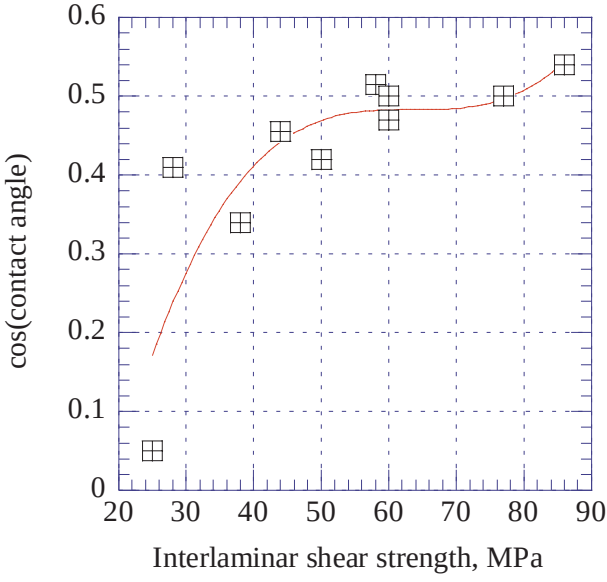

Figure 14.3. Contact angle of carbon fibers vs. interlaminar shear strength of epoxy composites. [Adapted, by permission from Tang L-G, Kardos J L, *Polym. Composites*, **18**, No.1, 1997, 100-13.]

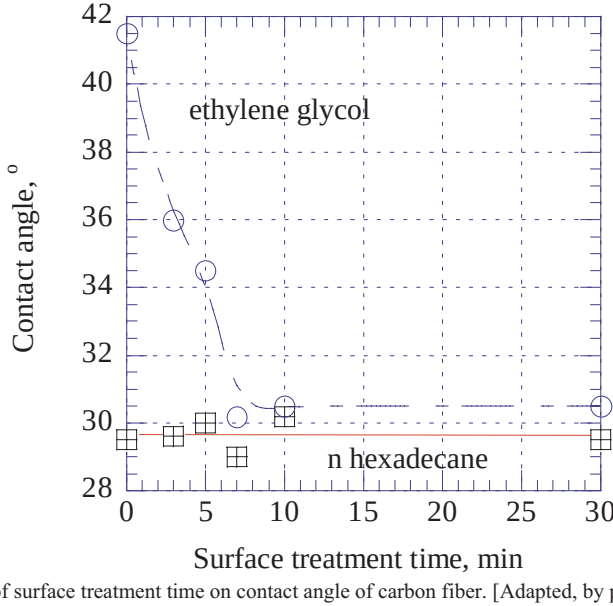

Figure 14.4. Effect of surface treatment time on contact angle of carbon fiber. [Adapted, by permission, from Ogawa T, Ikeda M, *J. Adhesion,* **43**, Nos.1-2, 1993, 69-78.]

ing a ground sample with pressure of 8 tones in a KBr die. A microsyringe deposits a droplet of water on the surface of a sample placed under optical microscope. The

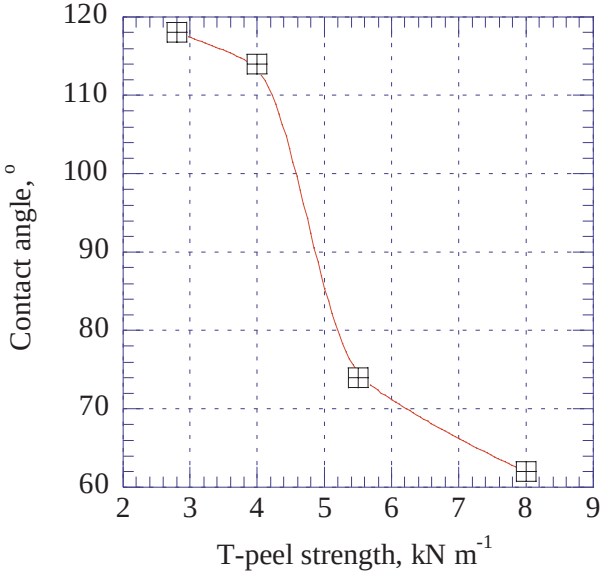

Figure 14.5 Contact angle vs. peel strength of SBR/polyurethane joints. [Adapted, by permission, from Torro-Palau A, Fernandez-Garcia J C, Orgiles-Barcelo A C, Martin-Martinez J M, *J. Adhesion*, **57**, Nos.1-4, 1996, 203-25.]

photograph of the droplet is taken and analyzed.[16] In the filler column method, contact angle is determined from liquid capillary rise.[14]

Standard methods: none

Major results: Figure 14.3 shows the effect of contact angle of carbon fibers on interlaminar shear strength of epoxy composites. An increase in contact angle of carbon fiber (e.g., increase in functional groups) results in an increase of interlaminar shear strength.[12] Figure 14.4 shows that the disperse component (relative to n-hexadecane) does not change with treatment time, whereas the polar component (relative to ethylene glycol) changes with time. The diminishing contact angle indicates that surface free energy increases, which is expected from the oxidation of carbon fiber.[17] Figure 14.5 shows that with a decrease of contact angle, peel strength of rubber polyurethane joints increases. The samples of rubber differ in silica content. The higher the silica concentration, the lower the contact angle and the higher the adhesion.[25] This is in correlation with SEM studies showing increasing surface roughening with increased addition of silica. The increase in surface roughness increases mechanical adhesion and thus improved peel strength.

14.1.7 DISPERSING AGENT REQUIREMENT[26]

Applications: The dispersing agent requirement is the minimum amount of dispersing agent required to produce a fluid dispersion of a particular carbon black loading. It is expressed as a weight percent of dispersant per total weight of carbon black. The dispersing agent requirement is an important parameter because a re-

duced amount of dispersing agent may cause instability of dispersion, whereas too large an amount of dispersing agent may restrict carbon black loading level and reduce weather stability.[26]

Testing procedure: Water is added to a blender, followed by ammonium hydroxide to adjust pH to the required level. Carbon black is added in 30 s with low speed mixing. Dispersing agent is added in portions from a burette under high speed dispersion. The endpoint is determined as 5 min of uninterrupted fluidity under high speed mixing. The total time of determination should not exceed 10 min.

Standard methods: The method is described in Cabot Corporation Technical Report S-131.

14.1.8 DISPERSION TESTS[27-30]

Applications: Considering that many properties of filled materials depend on the quality of dispersion, the reasons for conducting dispersion tests are self explanatory.

Testing procedure: There is no standard procedure applicable to all cases of filler dispersion because so many methods of processing are used for very diverse groups of materials. Some examples of tests used are given below. Carbon black is added to polymers processed by melting techniques for various reasons such as reinforcement, pigment, UV absorber, conducting additive, etc. Two tests are applicable to monitoring carbon black dispersion in these applications.[27] In one method, a pelletized masterbatch was processed in a Brabender Plasticorder PL-2000 single screw extruder equipped with a set of two screens (120×400 mesh which has a 45 μm rating and a second supporting screen of 24 mesh). A pressure transducer measured pressure versus time. The endpoint was either 400 s or a pressure exceeding 2000 psi. The results of the test were compared to a visual method in which a film extruded through a ribbon die, having dimensions of 75×0.24 mm, was used. The number of imperfections were correlated with the Plasticorder test. The distribution of fibers in a composite is measured by this method.[28] The radiation passes through the sample and a radiograph records the intensity of radiation transmitted through the object. The radiograph is then digitized to measure the intensity of each pixel, from which the distribution of each gray level within the image is determined. Based on the distribution of gray levels, it is possible to measure the local and average glass content. Other fillers such as carbon fiber were used with good results. Surface mapping was used to determine the degree of mixing of aluminum particles in polybutadiene.[29] The measurements were done by electron microscopy coupled with energy dispersive X-ray. In addition to filler dispersion, the preferred orientation was also determined.[29] In carbon black dispersions, four main methods are used: optical, microwave, electric conductivity, and dark field cut surface.[30] In the optical method, the image reflected from the cut surface is compared to standards and the nearest standard selected. The Dielecmeter (Sairem, France) is used in the microwave energy absorption method. The value of the dielectric constant depends

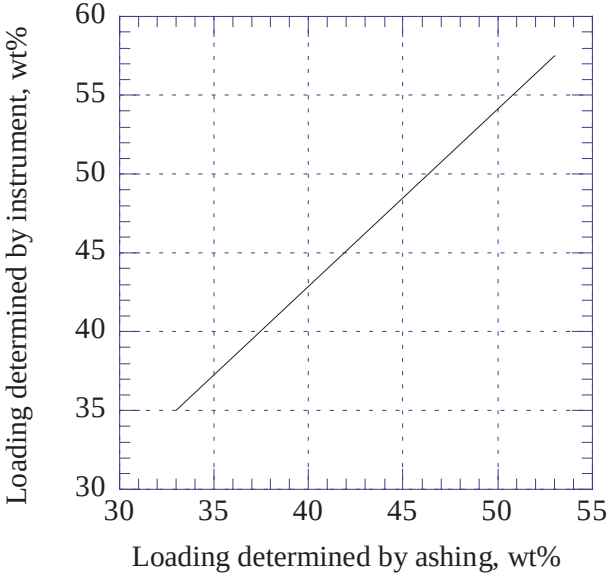

Figure 14.6. Glass loading determined by two methods. [Adapted, by permission, from Scott D M, *Composites, Part A*, **28A**, 1997, 703-7.]

on carbon black dispersion. Used in the electric conductivity method the Tangent Electroscanner (Tangent Scientific Instruments, Dublin, Ireland) has a measuring transducer with electrodes which induce alternating current in uncured rubber. The electrodes scan the surface of samples. The dark field cut surface method measures the light scattered from a cut surface, which depends on carbon black dispersion. Each method used for carbon black has some interference either related to the matrix in which carbon black is dispersed or to the conditions of running the experiment. This makes data difficult to compare.

Standard methods: ASTM D 2663, ISO 8780, ISO 8781, ISO 11420, ISO 13549

Major results: Figure 14.6 compares results of radiographic imaging with the ashing method. The data indicate that the method offers precise results.[28]

14.1.9 DRIPPING TEST[31]

Applications: The method is used to determine burning drops produced during material decomposition.

Testing procedure: The ignition source is a horizontal electric radiator producing a radiation intensity of 3 W/cm^2, positioned 30 mm above the specimen placed on a wire grid. 300 mm below the specimen, cotton wool is placed on receptacle for drops. If the specimen ignites during the first 5 min, the radiator is removed 3 s after ignition. During the second 5 min, the radiator is kept on regardless of whether the specimen burns or not. There are four classes - M.1 to M.4. If during the duration of test (10 min) the cotton wool ignites, the material is classified in class M.4. The assignment to the other classes depends on the amount of residues.

Standard methods: French specification NF P 92505
Major results: Huntite and hydromagnesite mixture at loading of minimum 25% in ethylene-propylene copolymers eliminates inflammation.[31]

14.1.10 DYNAMIC MECHANICAL ANALYSIS[32-34]

Applications: General method also used in filler applications. The results give information on mobility of molecules in the presence of filler, changes in the structure of the matrix due to interaction with filler, the effect of fillers on matrix degradation, microphase separation, and other related phenomena.
Testing procedure: DMA is mostly used as a scientific tool; therefore the testing procedure is selected depending on the requirements of the studies conducted.
Standard methods: none

14.1.11 ELECTRIC CONSTANTS DETERMINATION[35-42]

Applications: Fillers are essential components of formulations of materials which must have either electric conductivity, or high electric resistance, or EMI shielding capability. The addition of fillers to these compounds requires adequate methods of control.
Testing procedures:
ELECTRIC PROPERTIES
Dielectric properties. Dielectric constant and dissipation factor can be measured using a HP 4284A LCR meter with a HP 1645B test fixture.[37] The frequency range is 20 Hz to 1 MHZ. The dissipation factor is a measure of energy lost during the reversal of electric polarization. It is expressed as a fractional energy loss. The impedance bridge method is used to measure the dissipation factor, $\tan\delta$, dielectric constant (permittivity), ε', and dielectric loss factor, ε''. The configuration of electrodes and specimen painting with conductive paint is similar to the measurement of surface resistivity discussed below. The DC transient current method is an alternative method for the measurement of the dissipation factor and dielectric constants. In this method, a sample is charged with a constant voltage (e.g., 2 kV) for a long duration (e.g., 170 min). The specimen is then discharged. The charging and discharging currents are measured in short intervals (e.g., 5 s), and required constants are calculated.[41]
Electric resistivity. The electric resistance measurement is the same as discussed below under volume resistivity, to which this measurement is temporary adapted. For flexible materials, special electrode systems are developed to clamp sample and electric wires.[35] The measuring equipment is based on a Wheatstone bridge circuit. The conductivity of metal powder-containing epoxy was measured in special dies equipped with built-in brass electrodes inserted to the die. The material was cured in the die to assure good contact with electrodes.[36] Special sample holders and clamping devices are used for precise determination of rubber compounds containing carbon black.[39]

ELECTROSTATIC APPLICATIONS

Volume resistivity, surface resistivity, and charge decay time are major characteristics of electrostatic properties of materials. Volume resistivity, expressed in ohm-cm, is the resistivity of material measured on opposite ends of a material which is 1 cm thick. Surface resistivity, expressed in ohm, is a resistance between two electrodes placed along the same surface of the specimen. The charge decay time, expressed in s, is defined as the time needed to dissipate a certain percentage of charge induced on the surface of material. Other terms used include shielding effectiveness, decay half-time, peak voltage, and a percentage of charge retained. Shielding effectiveness, expressed in decibels, is a measure of attenuation of electromagnetic interference (EMI) by internal reflection, absorption, and partial reflection. Decay half-time, expressed in s, is the time to dissipate half the charge induced. Peak voltage, expressed in volts, is the maximum induced voltage in the charge decay test. The percentage of charge retained is a percentage of charge remaining in charge decay test after 500 s. The most frequently used methods of determining these quantities are characterized below. The respective standards are given in the next section.

Charge decay time. A specimen is placed in Faraday cage with electrodes on each side of the specimen. One electrode induces the charge, the other electrode measures changes in electric field. In this measurement, charge decay time, decay half-time, peak voltage, and the percentage of voltage remaining after 500 s are determined.

Surface resistivity. One side of the specimen is coated with a circle of silver paint surrounded by a ring of silver paint. The uncoated distance between the circle and the ring is an effective length on which surface resistivity is measured. The other surface of the specimen is fully coated with silver paint. Current and voltage are measured and surface resistivity calculated. If samples contain internal or external antistatics, the measurement is performed under a controlled atmosphere to eliminate the influence of temperature and relative humidity. Also, specimen conditioning is used to account for migration of the antistatic to the surface. The surface of specimen containing antistatics is not coated with silver paint, but electrodes are pressed to the surface. The resistivity of conductive pipes is determined in a special test arrangement.[38]

Volume resistivity. There are some differences between standard methods but the general principle is similar. A specimen of standard size is coated with a silver paint on the opposite surfaces to assure good surface conductivity. Two electrodes are attached to both surfaces in the manner minimizing contact resistance. The voltage applied depends on the expected resistance of the specimen and is in the range of 0.1 to 1000 v/mm thickness. Current and voltage are measured between the faces and volume resistance calculated. The edge effect can be minimized by means of guard electrodes.[37]

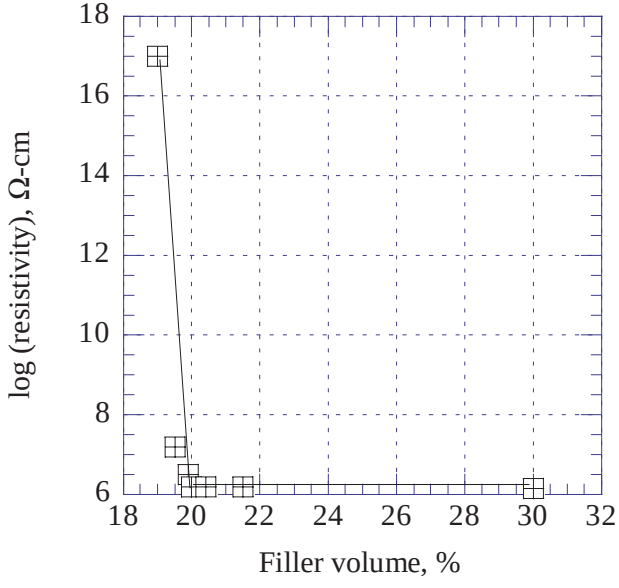

Figure 14.7. Resistivity of aluminum powder filled PMMA. [Adapted, by permission from Lei Yang, Schruben D L, *Polym. Engng. Sci*., **34**, No.14, 1994, 1109-14.]

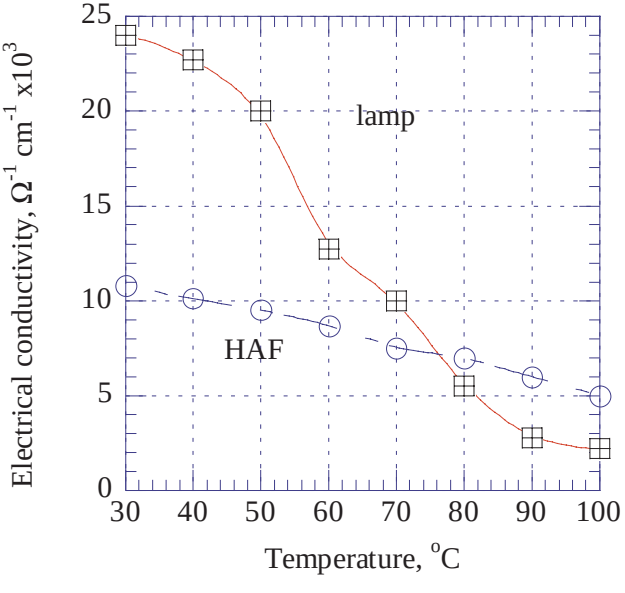

Figure 14.8. Conductivity of butyl rubber filled with carbon black vs. temperature. [Data from Nasr G M, Badawy M M, Gwaily S E, Shash N M, Hassan H H, *Polym. Degradat. Stabil.,* **48**, No.2, 1995, 237-41.]

Standard methods: electric resistance - ASTM D 257, shielding effectiveness - ASTM ES 7, BS 6667 (part 1 and 2), static decay - ASTM F 365, BS 2783 (part 2),

surface resistivity - ASTM D 25 (specimens containing antistatics), ASTM D 257, ASTM F 1173 (pipe resistivity), volume resistivity - ASTM D 257, DIN 53596, ISO 3915

Major results: Figure 14.7 shows that the resistivity of aluminum-filled PMMA changes abruptly. Smaller volumes of filler contribute a little to resistivity but, after certain threshold value of filler concentration, further additions have little contribution. A similar relationship was obtained for nickel powder; the only difference is in the final value of resistivity, which was lower for nickel due to its higher conductivity.[35] The same conclusions can be obtained from conductivity determinations of epoxy resins filled with copper and nickel.[36] Figure 14.8 shows the effect of temperature on the electric conductivity of butyl rubber filled with different grades of carbon black. In both cases, conductivity decreases with temperature, but lamp black is substantially more sensitive to temperature changes.[39] Even more pronounced changes with temperature were detected for the dielectric loss factor and dissipation factor for mineral filled epoxy.[41]

14.1.12 ELECTRON MICROSCOPY[43-59]

Applications: Electron microscopy as a general tool can be used in numerous applications in filled systems. The most frequent applications include: estimation of adhesion of fibers to the matrix in composites,[44] fracture mechanism of bone cements,[46] histological changes of bone cements and evaluation of the bone cement interface with glass fiber,[47] morphology of filler depleted layers of paint near the substrate,[48] morphology of fillers,[49] filler dispersion and distribution in the matrix,[51,53] filler aggregation after dispersion,[52,53,57] the effect of surface treatment on filler adhesion,[54] the effect of processing methods and flow patterns on filler distribution,[55] the effect of morphology and filler distribution on pyrolysis,[58] and structure of nanocomposites.[59] This broad list of applications shows the capabilities of the method in offering essential information on filled systems.

Testing procedure: SEM specimens are usually prepared for examination by prior sputtering with Au or Au-Pd alloys.[44,49] To enhance information, X-ray microanalyzers are used in combination to determine intensities of silicon, titanium, zinc, copper, calcium, nitrogen and phosphorus.[47,57,59] In TEM studies, electron energy loss spectra and element spectroscopic images are obtained, and the 3-window method is used for elemental studies.[57] Specimens are microtomed in a manner that does not distort the actual distribution of sample components. For example, fractured samples are microtomed below the fractured surface, left to relax, and then sputter-coated. Materials are frequently fractured under liquid nitrogen to obtain surfaces for filler distribution observation. In TEM studies, relatively high acceleration voltage is used (80 KeV), but samples are viewed at 120K to prevent degradation.[57] The highest magnification was used in TEM studies of nanocomposites where the smallest particle size of 2.9 nm was detected.[59] This analysis shows

that SEM and TEM are used in a fairly conventional manner for the analysis of filled specimens.
Standard methods: not applicable
Major results: The most interesting interpretation of SEM data regards technology of blend preparation, where electron microscopy permits monitoring of the stages of the process, and the effect of fillers on blend morphology, as well as following the effect of order of component addition on the properties of resultant material.[53] Application of SEM to industrial processing of filled plastics by different methods allows the understanding of the material flow pattern due to the orientation of particles of different sizes.[55] Combination of SEM or TEM with XPS is a very powerful technique. In paints, the cross-sectional distribution of filler in the proximity of coated substrate can be determined.[48] In nanocomposites, not only can particle sizes be measured, but also the chemical structure and morphology of these small particles obtained from mixed components can be determined.[59]

14.1.13 FIBER ORIENTATION[60-62]

Applications: Fiber orientation in composites or materials processed by other methods depends on processing parameters, characteristics of the fibers, and external stress applied to formed materials. Fiber orientation, on the other hand, affects mechanical performance and electric and thermal conductivity of fiber-containing material. This outlines the reasons for interest in fiber orientation determination.
Testing procedure: Microradiography is one method which allows the determination of fiber orientation.[60] Sample with a frozen-in fiber orientation is ground with abrasive paper of progressively finer grit sizes to 0.1-0.25 mm thickness. Soft x-ray white radiation was used to take images of microradiographs. These images were then processed by graphic software such as Adobe Photoshop and orientation determined by digitizing, followed by the determination of orientation function by numerical integration. In another study, orientation distribution function was determined according to a procedure discussed elsewhere.[62]
Standard methods: none
Major results: Figure 14.9 shows the fiber distribution angle for samples of glass fiber filled polyamide subjected to different levels of strain.[60] Micrographs (not included here) show that within this range of strains, fibers assumed orientations from the totally random (at $\varepsilon = 0$) to perfectly oriented (at $\varepsilon = 2.75$), which is very well reflected by the results of fiber orientation obtained from microradiographic studies.

14.1.14 FLAME PROPAGATION TEST[31,63]

Applications: The flame propagation test is used to classify materials into four categories from M.1 (nonflammable) to M.4 (highly flammable).[31] In aerospace applications, NASA uses the upward flame propagation test. This test simulates the beginning of a fire with a medium incident heat flux.[63]

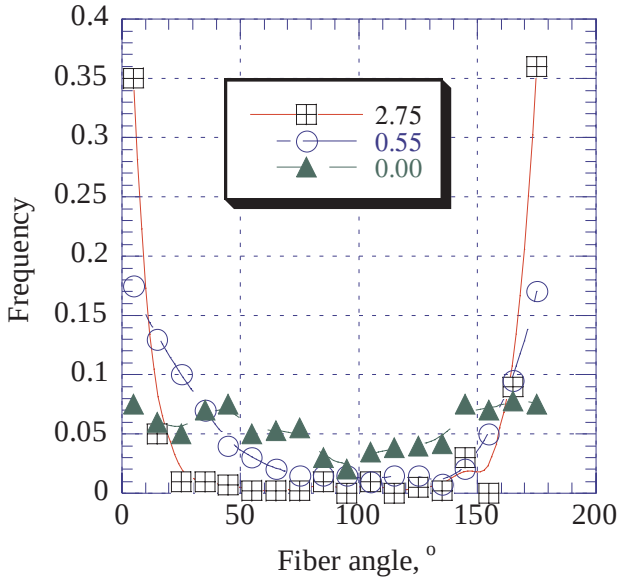

Figure 14.9. Fiber distribution at different strains. [Adapted, by permission, from Wagner A H, Kalyon D M, Yazici R, Fiske T J, Antec '97. Conference proceedings, Toronto, April 1997, 996-1000.]

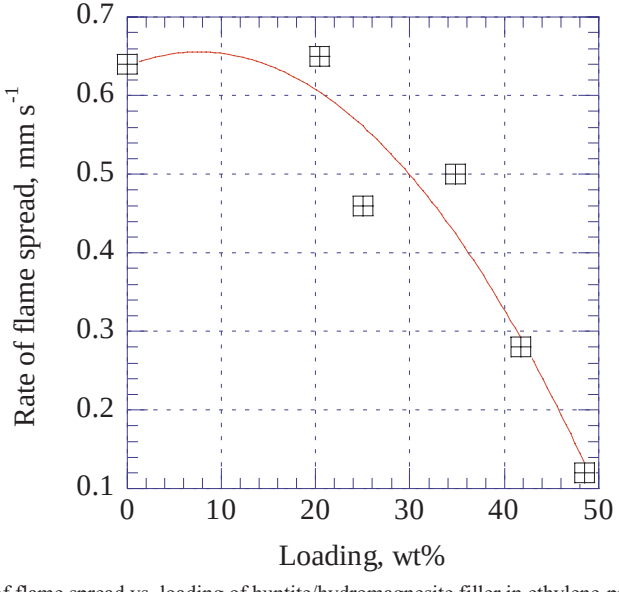

Figure 14.10. Rate of flame spread vs. loading of huntite/hydromagnesite filler in ethylene-propylene copolymer. [Data from Toure B, Lopez-Cuesta J, Benhassaine A, Crespy A, *Int. J. Polym. Analysis and Characterization*, , No.3, 1996, 193-202.]

Testing procedure: In the flame propagation test, the sample is clamped horizontally. Two marks are placed on the sample at a distance of 250 mm. A 50 mm space

is provided at the end of the sample for initiation of burning by a Bunsen burner. A time required to reach the second mark is determined, and from this time the rate of flame spread is calculated, expressed in mm/min.[31] The NASA upward propagation test is conducted in an atmosphere containing 30% oxygen. A sample 30.5 cm long is mounted vertically in a spring-clamp fixture. A chemical igniter is geometrically centered 0.64 cm below the front leading edge of the sample. The energy provided by a chemical igniter is 3128 joules and the total burn time of igniter is 25 s, with a flame height of 6.4 cm. The average flame spread rate is calculated by dividing the flame spread length by the flame spread time. The sample fails the test when the flame spread is greater than half the length of the sample.[63]
Standard methods: French specification - NF P 92-504; NASA Handbook 8060.1C test 1.
Major results: Figure 14.10 shows the effect of huntite/hydromagnesite loading on the rate of flame spread in ethylene-propylene copolymer.[31] A substantial decrease in the rate of flame spread is found when loading approached 50 wt%.

14.1.15 GLOW WIRE TEST[4]

Applications: Determination of minimum ignition temperature.
Testing procedure: The specimen is pressed against a tip consisting of a U-shaped wire coil heated by an electric current. The minimum ignition temperature is measured.
Standard methods: AS/NZS 4695, ASTM D 6194, BS EN 60695

14.1.16 IMAGE ANALYSIS[64-68]

Applications: Image analysis is a useful tool for many purposes of filler testing. Several examples of application exist in the current literature: the study of solid rocket propellant and liners by magnetic resonance imaging,[64] analysis of the behavior of polymers under extension,[65] surface deformation of polymer composites,[66] granulometry of short glass fiber in relationship to processing conditions,[67] and morphology of calcium carbonate filled polypropylene.[68] These and other applications of image analysis permit the transformation of image to numerical parameters, which can then be correlated to other factors of performance.
Testing procedure: There is no standard method used in these investigations, since requirements of image analysis must be synchronized with the method and geometry of material testing. At the same time, essential steps are similar, involving image acquisition, conversion of image to digital form, and analysis of the results. The image analysis becomes more complex if kinetic data must be obtained because of the rate with which the image must be captured, in order to free memory for the next image acquisition, and because of the method of further data processing. In magnetic resonance imaging, spin-echo and multislice pulse sequences were used for data acquisition. The resolution of imaging was $70 \times 70 \mu m$ and image size was 128×128 pixels. The data for each experiment were based on 48 scans giving a total acquisition time of 1.7 h for spin-echo and 0.85 h for multislice.[64] The method allows

the measurement of loading of filler and its distribution in the material, as well as the detection of voids and imperfections and the visualization of bubbles in the sample. The measuring system for the image analysis of behavior of polymers under large strains includes the following essential elements: camera, video recorder, frame grabber, array processor, time, and PC with large magneto-optical disk.[65] The array processor translates the image from analog to digital. The camera is initially activated by the signal from the tensile testing machine (first image), then subsequently by an electronic trigger which obtains the signal from the timer. A software program written in C language is capable of performing calculations of stress-strain-strain-rate behavior. The specimen for testing has a grid silk-printed on the surface to follow relative displacements of the grid and compare displacements with total draw force acquired from the load cell. This method consists of a measuring system capable of performing the determination without a physical contact with the sample. The use of image analysis in the measurement of scratch resistance is another important application.[66] The measuring system is used to analyze samples which were subjected to scratch testing prior to the optical analysis. The scratch surface is observed under crossed polarizers of an optical microscope at 100× magnification after placing them on a 360° rotating optical stage. The linearly polarized light reflected off the sample surface and a scattered light collected after passing through the crossed polarized analyzer is captured by a camera mounted on the top of the optical tube of the microscope and sent to an analog-to-digital converter. The digitized image for each pixel has gray scale values from 0 (black) to 255 (white) assigned. The result is then used to evaluate surface whitening of materials having different compositions (e.g., concentration of filler). The granulometric characterization of glass fibers for reinforced polypropylene was done by image analysis, which included image acquisition, image treatment, and quantitative analysis.[67] The fibers were dispersed in solvent between two glass slides (about 800 fibers) and observed with a polarizing microscope. Each selected fiber was labeled and captured images digitized. Using morphological tools, the image was filtered to improve quality and transferred into binary images. Software was used to calculate a size factor for each fiber which was then used to determine length distribution expressed by average number or average weight. In a similar application for particulate fillers, SEM images were digitized by an analog-to-digital converter.[68] Using Vidas software, the diameter, shape and orientation of particles were determined. From this review, it is concluded that image analysis methods are a very powerful (and easy to adapt) technology for gathering information on filler morphology in polymer systems. Recent developments in hardware will further contribute to the development of these methods and the understanding of real performance characteristics of fillers.

Standard methods: none

Major results: Figure 8.40 shows that the void density or whitening of talc filled polypropylene (relative to average scattering and scattering difference) increases

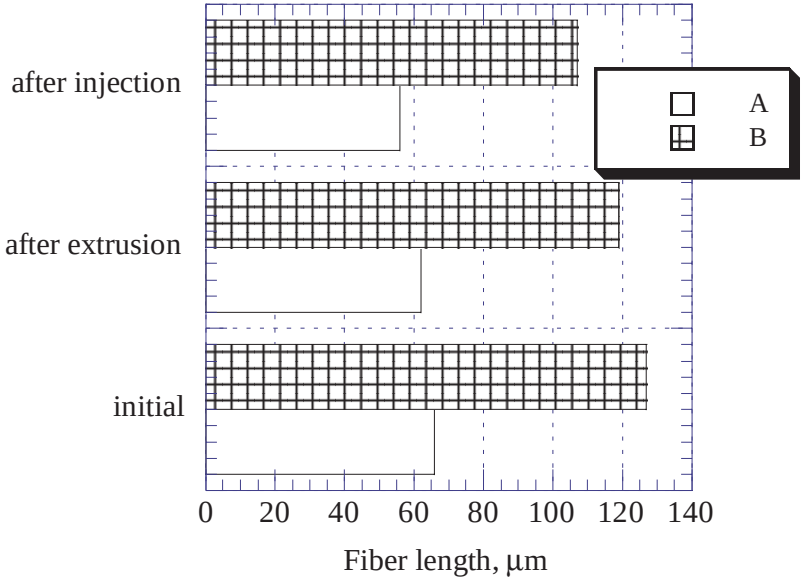

Figure 14.11. The average length of fiber prior to and after processing in glass fiber filled polypropylene. [Data from Averous L, Quantin J C, Lafon D, Crespy A, *Int. J. Polym. Analysis and Characterization*, **1**, No.4, 1995, 339-47.]

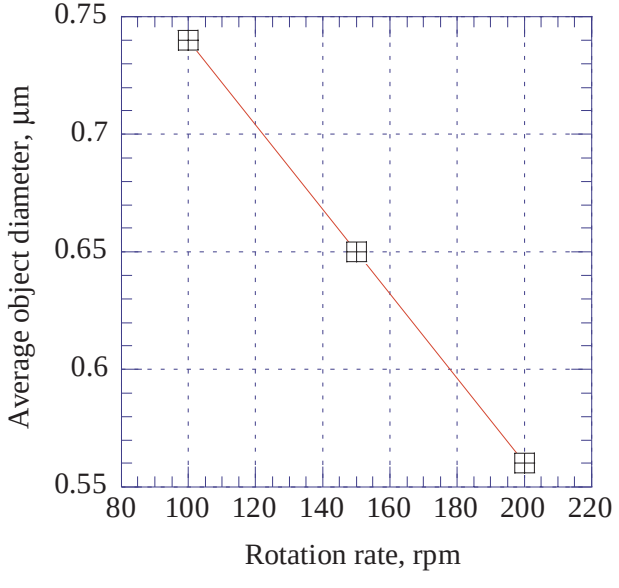

Figure 14.12. Average object diameter vs. rpm of Banbury mixer during incorporation of 10% calcium carbonate in polypropylene. [Data from Herzig R, Baker W E, *J. Mat. Sci*., **28**, No.24, 1993, 6531-9.]

(and scratch resistance decreases) with talc concentration increasing.[66] Fibers of different length distribution were used for extrusion and injection molding of glass

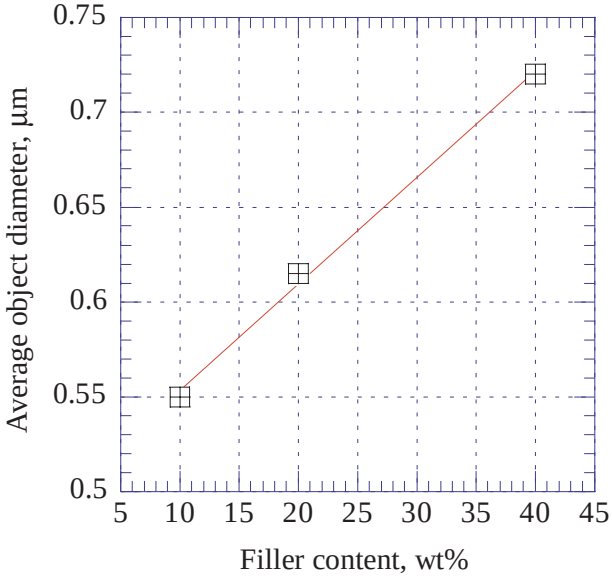

Figure 14.13. Average object diameter vs. $CaCO_3$ concentration after mixing in Banbury mixer with polypropylene. [Data from Herzig R, Baker W E, *J. Mat. Sci*., **28**, No.24, 1993, 6531-9.]

fiber reinforced polypropylene. The differences of average length of fibers after processing are given in Figure 14.11. Injection molding was more likely to cause changes in fiber length, but the loss of dimension was not large.[67] Figures 14.12 and 14.13 show the effect of mixing in a Banbury mixer on the object diameter (average particle size) of calcium carbonate in polypropylene vs. rpm and filler concentration, respectively.[68] Increased intensity of mixing contributed to particle size reduction whereas the increased concentration of filler caused particle size to increase.

14.1.17 LIMITING OXYGEN INDEX[4,31,63,69]

Applications: The test illustrates the relative flammability of materials by measuring the minimum concentration of oxygen in atmosphere required to initiate and support flame for more than 3 min.

Testing procedure: The minimum concentration of oxygen is measured using a vertically suspended sample in an instrument capable of modifying the atmosphere by mixing oxygen and nitrogen in required proportions (e.g., Stanton Redcroft instrument). The result of determination is presented in a form of % O_2.

Standard methods: ASTM D 2863, BS/ISO 4589, ISO 4589

Major results: Figure 14.14 shows that special fillers are required to increase the limiting oxygen index.[4] General fillers, such as talc, do not affect the limiting oxygen index in any other way than by dilution of the burning component (matrix). $Mg(OH)_2$, fire retarding filler, increases the limiting oxygen index along with a filler concentration increase.

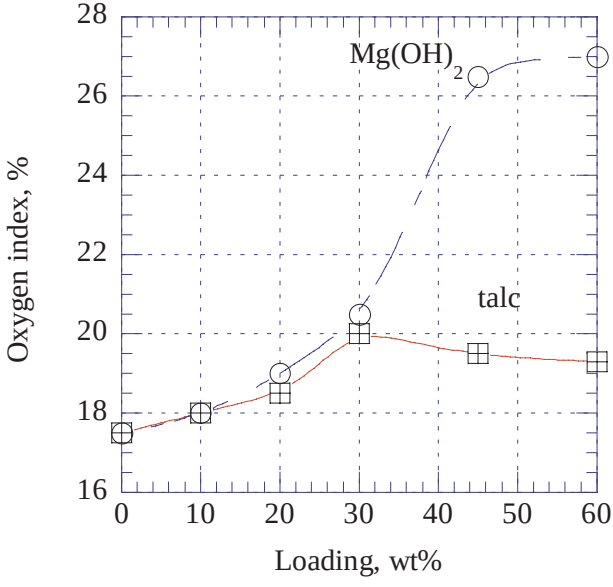

Figure 14.14. Limiting oxygen index vs. filler loading in PP. [Adapted, by permission, from Costa L, Camino G, Bertelli G, Borsini G, *Fire & Mat*., **19**, No.3, 1995, 133-42.]

14.1.18 MAGNETIC PROPERTIES[70,71]

Applications: Polymers are nonmagnetic materials but they can be modified by fillers. Plastic magnets, first introduced in 1955, are inferior to cast and sintered magnets but have many desirable properties such as low cost, ease of production, better uniformity and reproducibility.[70] Plastic magnets are used in electronic instruments, communication, household utensils, and audio equipment.

Testing procedure: The magnetic permeability measurement is performed on the samples formed to the shape of toroids wrapped uniformly with two sets of wire windings. The primary coil is excited with a sine wave from a function generator. The voltage induced in the secondary coil is measured with a lock amplifier at a frequency range of 0.5 Hz to 120 kHz.[70]

Standard methods: AS/DR 96526, ASTM A 772

Major results: In non-interacting spheres, the effective permittivity, $\varepsilon_{eff} = \varepsilon(1+3\phi)$, where ε is polymer permittivity and ϕ is filler fraction. Figure 14.15 shows that the use of ferromagnetic in LDPE gives substantially better performance.[70] The ferromagnetic filler, HyMu used in this study is composed of nickel, molybdenum, manganese, iron, and carbon. Nanocomposites containing magnetic fillers exhibit superparamagnetism and superferromagnetism. The nanocomposite materials can be changed by the choice of filler concentration because the interparticle distance controls the particle magnetization vector. Therefore, by changing interparticle distance (concentration), one may change properties from superferromagnetic to superparamagnetic at a given temperature.[71]

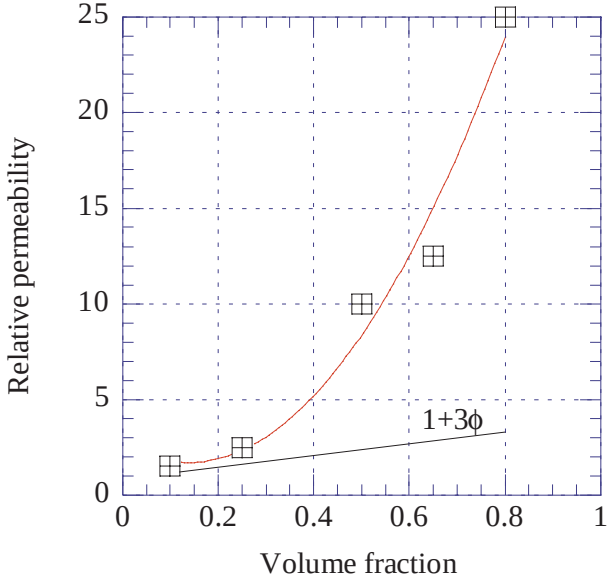

Figure 14.15. Magnetic permeability of LDPE filled with HyMu. [Data from Fiske T J, Gokturk H S, Kalyon D M, Antec '93. Conference Proceedings, New Orleans, La., 9th-13th May 1993, Vol. I, 614-7.]

14.1.19 OPTICAL MICROSCOPY[50,53]

Applications: Optical microscopy finds several important applications in filled systems, including observation of crystallization and formation of spherulites[50] and phase morphology of polymer blends.[53] In the first case, important information can be obtained on the effect of filler on matrix crystallization. In polymer blends, fillers may affect phase separation or may be preferentially located in one phase, affecting many physical properties such as conductivity (both thermal and electrical) and mechanical performance.

Testing procedure: In crystallization studies, samples are placed on a hot stage of a polarizing microscope and crystallization regime (cooling) is strictly controlled. The photomicrographs show the stages of the crystallization and the morphology of spherulites.[50] The effect of temperature, up to the melting point, and the cooling rate on blend morphology can also be observed using a hot stage.[53]

Standard methods: not applicable

Major results: Carbon black has a better affinity to polyamide than polypropylene. Even if carbon black was added to polypropylene, it was preferentially transferred to the polyamide phase during mixing.[53] In a polymer blend of two polymers, polyamide formed the minor phase and, due to preferential location of carbon black in its phase, the carbon black concentration in the polyamide phase was much higher than expected from the amount of carbon black added. This high concentration of carbon black in the minor phase resulted in substantially increased conductivity of the blend.[53]

14.1.20 PARTICLE SIZE ANALYSIS[31,72,73]

Applications: The particle size distribution of filler is one essential parameter controlling the performance of filled materials and as such it is a control parameter of commercial fillers.
Testing procedure: The most crude method of analysis of particle size distribution is based on sieve analysis. Considering that most fillers contain very small particles, this method is usually inadequate for practical purposes. A Coulter counter is a common instrument used to determine particle size distribution.[31] Particles of filler suspended in water are measured by laser diffraction and recalculated to distribution by volume or weight. Various surface phenomena may affect the readings but still this is one of the most suitable methods of measurement. The measurement of particle size of carbon black is very difficult. The best results are obtained by TEM,[72] but here also very high irregularity of the carbon black shape makes the measurement not very reliable. The particle size of carbon black is frequently correlated with a specific surface area measured by BET method. This again has many other influences considering that carbon black is energetically heterogeneous, and adsorption of gas or liquid depends on functional group concentration.[73] Studies of oxidized carbon black indicated that the specific surface area of carbon black changes on oxidation whereas TEM determined size does not. Determination of the structure of carbon black is even more difficult and results are confusing. It can be summarized that, in spite of the fact that particle size analysis is very important, there is a great deficiency in techniques available to measure it.
Standard methods: AS 2879, ASTM D 3360, ASTM D 3849, DIN 66111, ISO 4497

14.1.21 RADIANT PANEL TEST[69]

Applications: In this test, the flammability of materials is considered as a function of the heat release rate and critical ignition energy. Flammability is inversely proportional to ignition energy and directly proportional to heat released.[69]
Testing procedure: The test sample is exposed to heat from a radiant panel at a 30^{o} angle, meaning that the upper portion is severely exposed. The time progress of ignition down the specimen is the so-called flame spread factor. The thermocouples placed above the specimen serve as a heat-flux measuring device to monitor the rate of heat release, called a heat evolution factor. The two measurements multiplied by each other give a flame spread index. Two materials are used as calibrating specimens. The mineral hardboard with an index 0 and red oak with index 100 serve as calibrating specimens.[69]
Standard methods: ASTM E 162, ISO/DIS 13927

14.1.22 RATE OF COMBUSTION[4]

Applications: Flammability of filled systems.
Testing procedure: Horizontally held specimen is ignited at one end. The rate of combustion is calculated from the time required for the flame to pass a 25 mm

length. If the flame is extinguished before the 25 mm mark, then an arbitrary zero rate is given to the specimen.
Standard methods: AS 2122, ASTM D 635
Major results: Figure 12.8 shows that talc increases the rate of PP combustion whereas $Mg(OH)_2$ used in sufficient concentration decreases the combustion rate.[4]

14.1.23 SCANNING ACOUSTIC MICROSCOPY[74]

Applications: Nondestructive method of determination of carbon fiber reinforced composites. Damage of woven fiber reinforced composites, distribution of filler due to flow in molding techniques, distribution of fiber in composite, and dispersion of carbon black are examples characterizing potential applications of the method.[74]
Testing procedure: A sapphire rod with a concave spherical surface at one end and an epitaxially grown piezoelectric transducer on the other end form the acoustic transducer which is the most essential element of the acoustic microscope. A transmitter supplies the RF signal to the transducer. The signal is converted into acoustic waves which propagate through the rod. The sample is scanned and the acoustic wave at each point is reflected back to the transducer acting as receiver. The transducer converts the acoustic wave to an RF signal, which is then translated to the electrical voltage corresponding to the amplitude measurement. This is then stored as a digital value in memory. When scanning is completed, the acoustic properties of the specimen are converted to a gray scale and displayed on a monitor. Samples are examined either by pulse or burst modes. The pulse mode, operating at a lower frequency, is suited for in-depth examination of materials (up to several mm). The instrument responds to either discontinuity in a sample (cracks, voids, delaminations) or changes in properties (inclusions, fibers, crystalline structures). The burst mode operates at a high frequency range which allows for much higher resolution. The method is capable of generating an image of the subsurface and operates about 500 μm below the surface.
Standard methods: not applicable
Major results: The method is useful for control of expensive materials in responsible applications, such as, for example, materials used in aeronautics. Material control or inspection can be conducted (pulse method) without damage caused to the inspected material. The other essential advantage of the method is related to the fact that fillers can be observed within the filled material, which is not possible by any other technique. In addition, clarity of the micrograph is improved compared with optical microscopy. This method, although unique, has many applications in filled materials and hopefully more data will be known in the future in order to facilitate better understanding of filled materials.

14.1.24 SMOKE CHAMBER[4,69]

Applications: Smoke evolution of commercial materials and the effect of various additives including fillers on smoke production rate.

Testing procedure: An NBS smoke chamber is equipped with six flamelet burners and a radiant heat source. Non-flaming samples are tested using the heater alone. The sample is placed vertically in a front of the heater (2.5 W/cm^2). The results are obtained by measuring the percent transmission of a light beam which travels from the bottom of the chamber, through the smoke, to the photomultiplier tube at the top. The results are recorded as a function of time. The transmittance measured is converted to the specific optical density from the following equation: $Ds = V\left[\log(100/T)\right]/LA$, where V is chamber volume, L is the light beam path length, A is the sample area, and T is the transmittance.
Standard methods: ASTM E 662
Major results: General fillers do not affect smoke formation by any means other than simple dilution. Fire retardant fillers such as $Mg(OH)_2$ decrease smoke formation only at high concentrations.[4] Materials which are known catalysts of degradation (e.g., copper) increase smoke formation.[69]

14.1.25 SONIC METHODS[75-78]

Applications: The physical principle of measurement is similar to the scanning acoustic microscopy discussed in the Section 14.23, but applications and the method of data processing are essentially different. Sonic methods were used in the following applications to filled materials: the effect of particle size and surface treatment on acoustic emission of filled epoxy,[75] longitudinal velocity measurement of tungsten filled epoxy,[76] and in-line ultrasonic measurement of fillers during extrusion.[77] Numerous parameters related to fillers can be characterized by this non-destructive method.
Testing procedure: A sample in the form of dumbbell was tested in a tensile testing machine with an acoustic emission transducer attached to its surface using silicone grease and vinyl tape. The acoustic emission generated during tensile testing was analyzed.[75] The velocity of ultrasonic waves traveling in the material under test was used for the determination of longitudinal and shear moduli.[76] The experimental setup included a sample, transmitting transducer, and receiving transducer all immersed in water to improve propagation of acoustic waves. The transmitting transducer was connected to the acoustic wave generator and the receiving transducer to an oscilloscope. The bulk modulus and shear and Young's moduli were calculated from longitudinal velocity.[76] In extruder experiments,[77] the emitting and receiving transducers were installed on the die wall so as to not interfere with the flow of polymer. The attenuation was measured in this experiment because ultrasonic velocity is temperature and pressure dependent.
Standard methods: not applicable
Major results: Figure 14.16 shows the effect of mean particle size of spherical silica (flame-fused synthetic silica) on acoustic emission. The emission increases with the particle size of filler increasing.[75] The source of this increase in acoustic emission is thought to be related to the fracture of particles, debonding of particles from

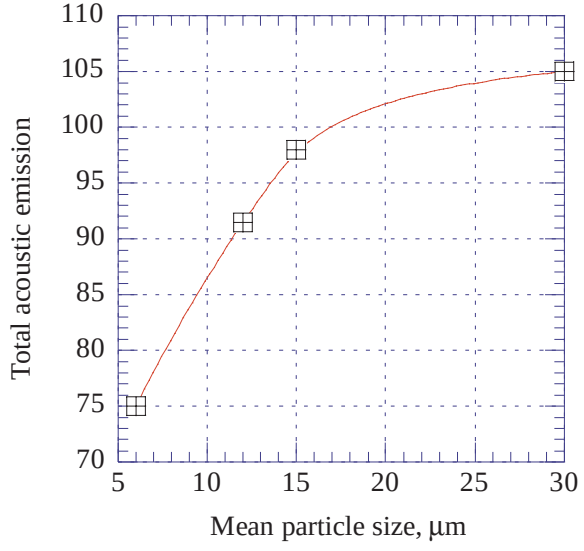

Figure 14.16. The effect of mean particle size of silica on total acoustic emission of epoxy filled with 70% silica. [Data from Ohta M, Nakamura Y, Hamada H, Maekawa Z, *Polym. & Polym. Composites*, **2**, No.4, 1994, 215-21.]

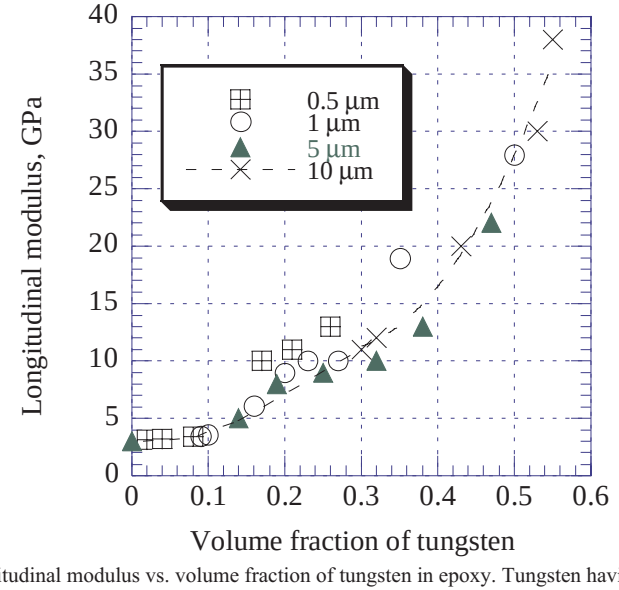

Figure 14.17. Longitudinal modulus vs. volume fraction of tungsten in epoxy. Tungsten having particle sizes from 0.5, 1, 5, and 10 µm is plotted on the graph. [Adapted, by permission, from Nguyen T N, Lethiecq M, Levassort F, Patat F, *Int. J. Polym. Analysis and Characterization*, **1**, No.4, 1995, 277-87.]

the matrix, and cracks formed in the matrix. The tensile strength of the composite decreased with increasing particle size which is in agreement with interpretation. Figure 14.17 shows that the longitudinal modulus increases with addition of tung-

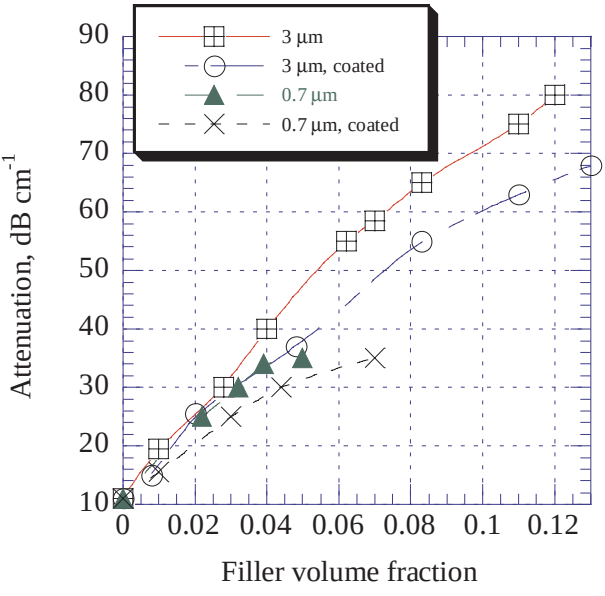

Figure 14.18. Attenuation vs. volume fraction of different fillers. [Adapted, by permission, from Gendron R, Daigneault L E, Tatibouet J, Dumoulin M M, Antec '94. Conference Proceedings, San Francisco, Ca., 1st-5th May 1994, Vol. I, 167-71.]

sten increasing.[76] The particle size in the measuring range has very little effect on modulus. In extrusion experiments, acoustic measurements were used to measure the distribution of residence time in the extruder.[77] This method is an alternative solution to the normal practice of such measurements, which consists of the addition of dye to the extruded compound to evaluate the quality of mixing. A filler ($CaCO_3$ in this experiment) can be used as tracer. Figure 14.18 shows the effect of filler grade on attenuation. Camel-Wite has an average particle size of 3 µm and Camel-Cal of 0.7 µm. Both grades were tested with and without stearic coating. It is noticeable that larger particles give stronger signals (more imperfections) and uncoated grades also give stronger signals (more difficult to disperse). Increasing volume fraction of filler contributes to the increase of attenuation. $CaCO_3$ was found to be a very suitable choice for application (as a tracer to measure residence time required).[77]

14.1.26 SPECIFIC SURFACE AREA[78]

Applications: Determination of specific surface area of filler which is used as a factor relative to particle size, porosity, and surface activity of filler.

Testing procedure: The automated instruments (e.g., Quantachrome NOVA 1000 or Micrometrics Gemini 2360) are used for rapid surface determination. The physical adsorption of nitrogen or other inert gas should be conducted at a pressure which is within the range of linearity.

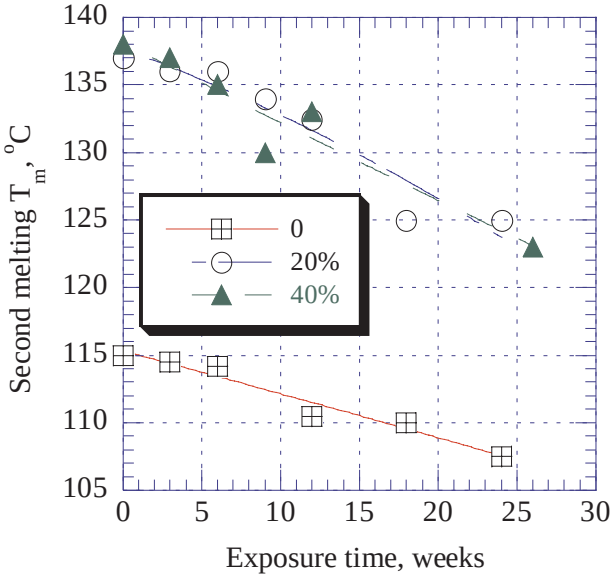

Figure 14.19. Crystallization temperature of talc filled PP vs. UV exposure time. [Adapted, by permission, from Rabello M S, White J R, *Polym. Composites*, **17**, No.5, 1996, 691-704.]

Standard methods: ASTM C 1069, ASTM D 1993, ASTM D 5604, BS 4359: Part 1, ISO 9277

14.1.27 THERMAL ANALYSIS[50,52,79-98]

Applications: Thermal analysis found numerous applications in filled systems. The following studies were conducted: the effect of filler on degradation rate of HDPE,[50] mechanism of degradation of PU foams filled with inorganic flame retardants,[82] thermal degradation of ethyl acrylate copolymer in the presence of fillers,[87] photodegradation of filled polypropylene,[89] the effect of nucleating filler on the photodegradation of polypropylene,[85] the effect of cooling rate on crystallization of HDPE in the presence of fillers,[50] dynamic mechanical analysis of nanocomposites,[52] determination of glass fiber content in a composite,[70] cure kinetics in the presence of fillers,[80] activation energy of curing in the presence of fillers,[90] the effect of filler on the curing kinetics of a composite,[91] glass transition temperature at different filler contents,[81] glass transition temperature of nanocomposites containing whiskers,[88] thermal degradation of polymer blends containing fillers,[92] thermal decomposition of fillers,[94] the effect of filler loading on DTA of filled polymer,[95,96] and formation of an interpenetrating network in the presence of filler.[97]

Testing procedure: Testing of thermal properties is a fairly standard procedure which is not discussed here. DSC was used for the studies on the effect of cooling rate on formation of spherulites in the presence of fillers.[50] In order to assure the repeatability of conditions of the experiment, the instrument was calibrated with indium and tin standards.[50] The TGA/DSC instrument was coupled with a mass

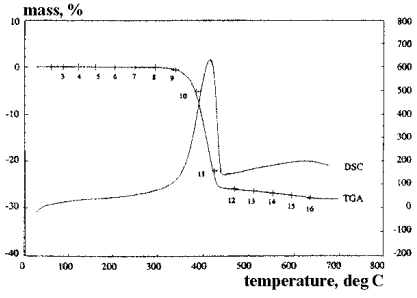

Figure 14.20. TGA curve for $Mg(OH)_2$. [Adapted, by permission, from Hornsby P R, Wang J, Rothon R, Jackson G, Wilkinson G, Cossick K, *Polym. Degradat. Stabil.*, **51**, No.3, 1996, 235-49.]

spectrometer and FTIR and gases released from thermal decomposition analyzed for composition.[94] In most cases, the thermal analysis was used in a standard way.

Standard methods: not applicable

Major results: Figure 14.19 shows that the crystallization temperature of filled PP is substantially higher than for unfilled polymer.[89] There is no difference in crystallization temperature between 20 and 40% talc. It was reported in the literature that only a small addition of talc increases the crystallization temperature due to nucleation. A further increase in talc concentration does not change crystallization temperature. UV exposure of talc filled PP changes the affinity of PP to talc causing a gradual drop in crystallization temperature. Figure 14.20 shows the thermal decomposition of $Mg(OH)_2$.[94] The water release is accomplished within a temperature range of 320 and 440°C. It was determined by DSC that the reaction is strongly endothermic.

14.2 CHEMICAL AND INSTRUMENTAL ANALYSIS

14.2.1 ELECTRON SPIN RESONANCE[99-101]

Applications: ESR spectroscopy was used to monitor the orientation and distribution of filler particles in polymer composites,[99-101] and molecular movement in filled, crosslinked material was studied.[100]

Testing procedure: Free radicals were generated by γ-irradiation from a cobalt source at -75°C. The radical decay study was performed at 40°C.[100] Most inorganic fillers contain paramagnetic impurities and defect centers in their crystalline structure. The orientation of the magnetic axis of these paramagnetic centers can be characterized by ESR.[99] By measuring the magnetic anisotropy of naturally occurring Mn(II) centers in calcium carbonate and in talc the change in orientation of the filler can be followed.[101] The amplitude ratio of characteristic ESR bands gave the order parameter.

Standard methods: not applicable

Major results: Figure 14.21 shows the effect of the concentration of silica filler on radical decay in a crosslinked and uncrosslinked system.[100] Both fillers and crosslinks restrict molecular mobility. A small addition of filler has a very large effect on radical decay (and molecular mobility). Further addition of filler has a decreased effect on the rate of radical decay.[100] The orientation of the particles changed as a function of composition, depending on processing technology (the type of molding, i.e., injection versus compression molding), and had a specific spatial distribution in the cross-section of the injection molded specimen. A

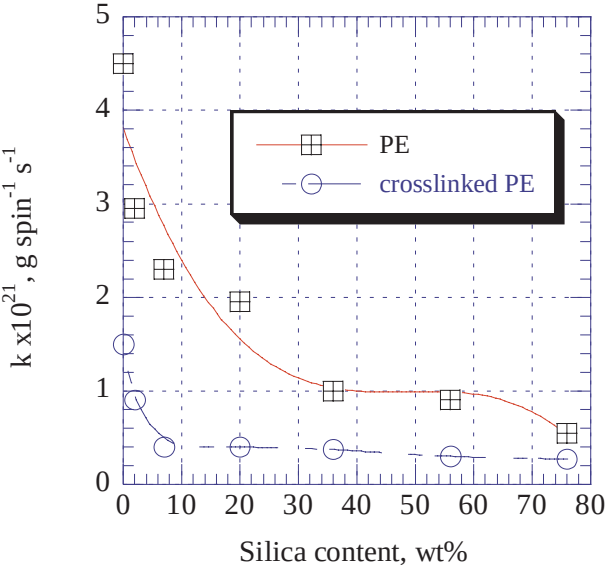

Figure 14.21. Rate constant of free radical decay at 40°C vs. content of silica in PE. [Adapted, by permission, from Szocs F, Klimova M, Chodak I, Chorvath I, *Eur. Polym. J.*, **32**, No.3, 1996, 401-2.]

correlation was found between average orientation of anisotropic particles and the mechanical properties of various composites.

14.2.2 ELECTRON SPECTROSCOPY FOR CHEMICAL ANALYSIS[102-106]

Applications: ESCA was used in studies of polyurethane containing metal salts,[102] to determine the distribution of silica in a PVA matrix,[103] to analyze surface groups of carbon black,[104,105] and to observe the effect of surface modification on the surface composition of composites.[106]

Testing procedure: Standard methods of sample preparation and instrument operation are used.

Standard methods: not applicable

Major results: The analysis of ultrafine particles in polyurethane shows that Ni^{2+} was reduced in the process to metallic Ni. After 15 days, some Ni atoms on the surface were oxidized, but the Ni atoms residing in the bulk were not affected by oxidation.[102] The differences in concentration between the front and the back of the sample of PVA containing silica were -4, +2, and +2 for C, O, and Si, respectively.[103] This shows good intermixing between polymer and filler. At the same time, the values for all three atoms do not match the theoretical values, which is attributed to the reaction between unreacted ethoxide groups and silica forming covalent bonds.[103] Substantial differences between furnace carbon black and carbon black obtained from the pyrolysis of tires were detected by ESCA.[104] Furnace carbon black had one strong graphitic carbon peak and very small peaks of carbon-

oxygen and carbon in aliphatic or aromatic compounds. Carbon black from pyrolized tires had strong peaks of all compounds.[104] Treatment of carbon black by plasma changes the concentration of atoms on the surface of carbon black, but heating these treated samples at 900°C returns them to the initial composition.[105] The concentration of several groups was studied, including C-C, C-O, C=O, COO, keto-enol, and C-NH_2.[105]

14.2.3 INVERSE GAS CHROMATOGRAPHY[15,18,19,72,93,105,107-116]

Applications: Inverse gas chromatography became one of the most important tools used for studying the surface properties of fillers. The following information can be obtained from measurements: isotherms of adsorption of various probes, energy distribution of adsorption, heat of adsorption, surface free energy, dispersive (nonpolar) component of surface energy, polar contribution to surface energy, specific components of the free energy of adsorption, enthalpy and entropy of adsorption, acid-base forces (pair interaction parameter), work of adhesion between polymer and filler. The fillers for the following applications were studied by inverse gas chromatography: the effect of plasma treatment of carbon black,[105] the effect of thermal treatment of carbon black on rubber reinforcement,[18] heats of adsorption of various probes on carbon black,[72] the effect of compression on surface activity of carbon black,[19] the effect of extraction on the properties of carbon black,[110] properties of commercial carbon blacks,[111] the effect of filler surface energy on its performance in paints,[15,108] acid/base properties of fumed silica used in silicone elastomers and silica modification by thermal treatment,[109] surface properties of ZnO and their effect on the reinforcement of elastomers,[112] acid/base properties of $CaCO_3$,[113] characterization of Kevlar fibers,[114] heterogeneity of the filler surface,[115] and the effect of fillers in polymer blends.[116] Reversed-phase liquid chromatography is based on a similar approach but it is not as broadly applied as inverse gas chromatography.[107]

Testing procedure: The principle of measurement by inverse gas chromatography is similar to gas chromatography, in which the instrument contains a column placed inside the thermostated chamber, an injection port and a detector. The injected sample, carried through the chromatographic column by a carrier gas, is separated on a stationary phase of column, and measured by detector. In gas chromatography, the stationary solid phase is selected to give the best separation of mobile vapor phase. In inverse gas chromatography, the mobile vapor phase is a probe selected from numerous polar and nonpolar liquids and the stationary phase is composed of filler (or polymer) under testing. The method can be used to characterize independently filler and polymer particles and to analyze polymer-filler interaction. A large body of theoretical treatment of data exists which allows the calculation of numerous parameters listed in the *Applications*. The peculiarity of equipment operation in inverse gas chromatography in comparison to standard gas chromatographic measurements is related to the preparation of the column, which may introduce

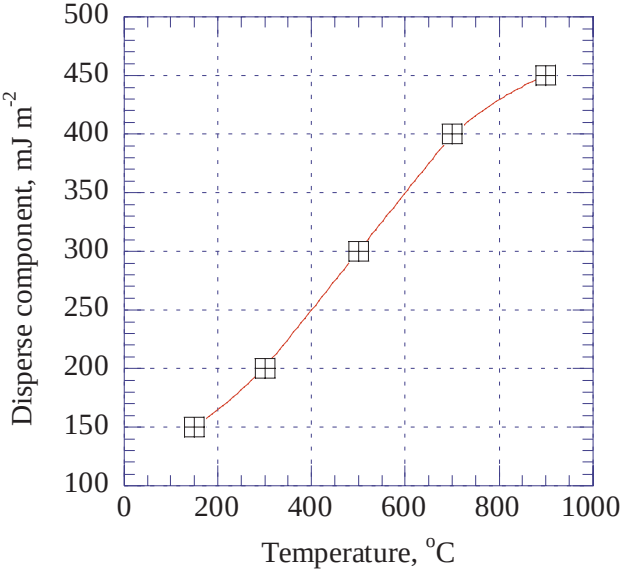

Figure 14.22. Disperse component of carbon black vs. temperature of thermal treatment under nitrogen. [Adapted, by permission, from Donnet J B, Wang W, Vidal A, Wang M J, *Kaut. u. Gummi Kunst*., **4**6, No.11, Nov.1993, 866-71.]

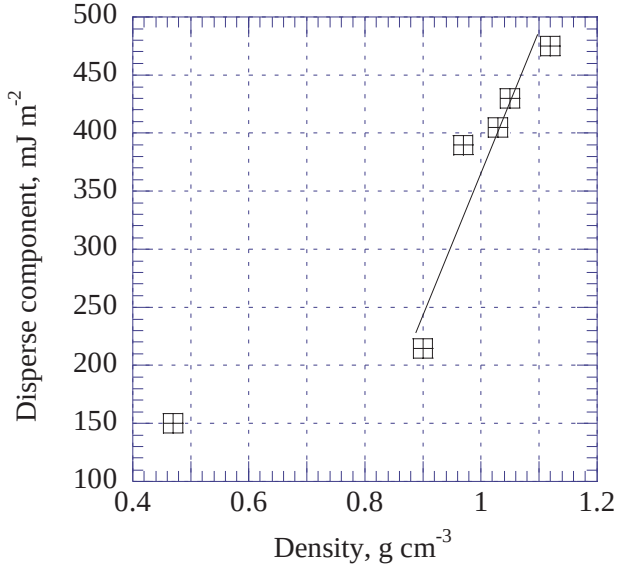

Figure 14.23. Disperse component vs. density of carbon black on compression. [Adapted, by permission, from Wang W D, Haidar B, Vidal A, Donnet J B, *Kaut. u. Gummi Kunst*., **47**, No.4, 1994, 238-41.]

measurement error. In gas chromatographic measurements, the stationary phase is very well defined if purchased from a reputable supplier. In inverse gas chromatography, the column is prepared by the user with material which was not optimized

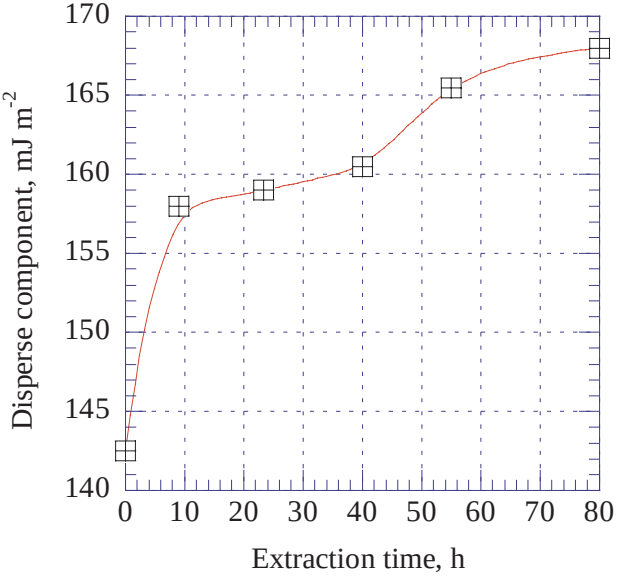

Figure 14.24. Disperse component vs. extraction time of carbon black by boiling toluene. [Adapted, by permission, from Vidal A, Wang W, Donnet J B, *Kaut. u. Gummi Kunst.*, **46**, No.10, 1993, 770-8.]

for unrestricted flow. The material for analysis has to be prepared in such a manner that a negligible flow rate drop occurs when carrier gas passes through the column. In one study,[109] fumed silica powders were agglomerated by dispersing in hexane, allowed to dry under nitrogen and sieved through a wire mesh to obtain a narrow distribution of particle sizes. Similar procedures are used in carbon black studies.[110] It should be pointed out that the method of preparation of material should also not alter surface properties of filler, since it can change the results of measurements. It is also essential to condition a column especially if surface-modified fillers are used, to remove a chemical load which otherwise will affect the conditions of adsorption and detection. Infinite dilution is one essential modification of measurement. In this case, very small samples of probes (close to the detection limit of detector) are injected.[112] Dead volume of a column is minimized by close packing[114] and measured by injecting methane.[112]

Standard methods: none

Major results: Many examples are available in the current literature concerning how this method can enhance understanding of the use of fillers. Figure 14.22 shows that the dispersive component of carbon black increases with temperature of treatment under nitrogen.[18] About half of the acid groups disappear at 500°C, and they all disappear at 900°C.[18] At around 700°C, the dispersive component begins to reach a plateau. This suggests that the surface chemical groups at the lowest oxygen containing positions do not play a positive role in the increase of surface energy and explains why polymer-carbon black interaction decreases upon oxidation of filler.

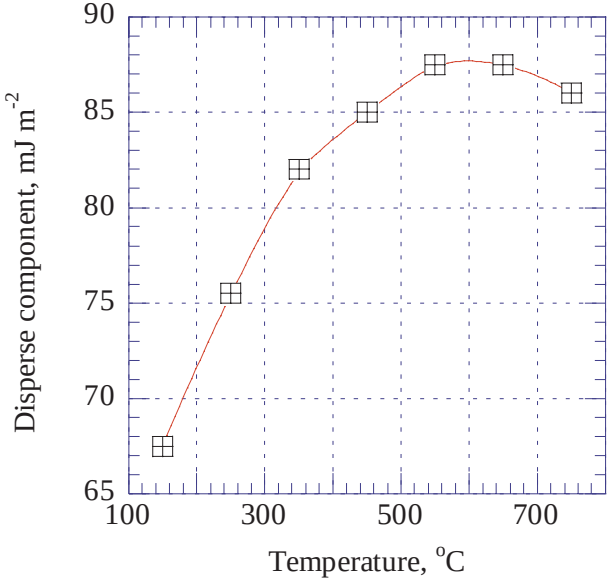

Figure 14.25. Disperse component of fumed silica vs. temperature of thermal treatment. [Adapted, by permission, from Zumbrum M A, *J. Adhesion*, **46**, Nos.1-4, 1994, 181-96.]

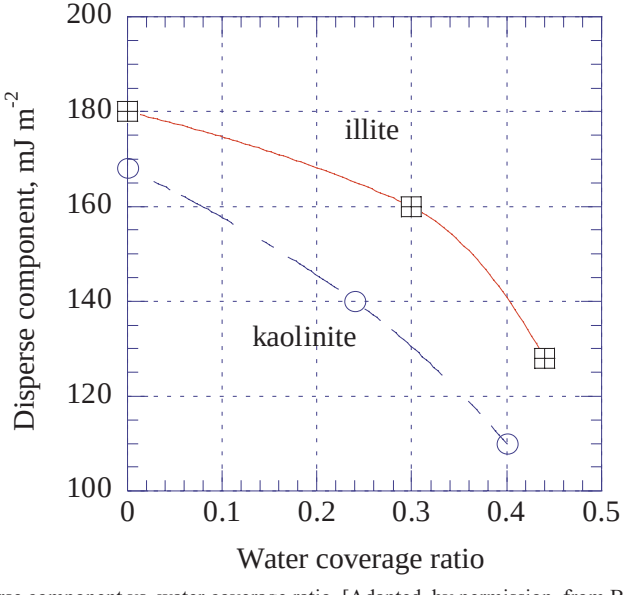

Figure 14.26. Disperse component vs. water coverage ratio. [Adapted, by permission, from Balard H, Saada A, Hartmann J, Aouadj O, Papirer E, *Macromol. Symp*., **108**, 1996, 63-80.]

Densification of carbon black by compression increases the dispersive component of surface free energy.[19] This process is initially not proportional to density, but after some threshold value at around 0.7 g/cm^3 the dispersive component has a linear

relationship with density(Figure 14.23). Also, extraction of carbon black with solvents increases dispersive component due to elimination of certain functional groups from the surface (Figure 14.24).[110] The thermal treatment of fumed silica also results in an increase of the dispersive free energy due to condensation of adjacent silanol groups (Figure 14.25).[109] Figure 11.2 shows the effect of acidic and basic calcium carbonates on elongation.[113] Water adsorbed on the filler surface decreases the dispersive component due to shielding of the sites having the highest adsorption energy (Figure 14.26).[115]

14.2.4 GAS CHROMATOGRAPHY[92,117,118]

Applications: Gas chromatography has limited applications to filled systems. It was used for characterization of the various degradation products of ethylene ethyl acrylate copolymer filled with calcium carbonate by GC-MS,[92] evaluation of ecotoxicological properties of materials containing flame retardants,[117] and determination of carbon black content by pyrolysis gas chromatography.[118]
Testing procedure: Volatile products of degradation were absorbed in Tenax cartridges and the ethanolic eluate of the Tenax cartridge was analyzed by GC-MS.[117] The furnace type pyrolyzer was connected to the gas chromatograph, and pyrolysis was conducted under helium. Volatiles were used for the identification of polymer and residue to determine the amount of carbon black.[118] The standard error of determination of carbon black was in the range of 0.2 to 3.4%.
Standard methods: not applicable
Major results: Calcium carbonate prevents formation of acids by interacting with acid groups.[92] Products of higher molecular weight are produced in the presence of filler.

14.2.5 GEL CONTENT[119,120]

Applications: Determination of the insoluble fraction of polymer in compounded and processed materials.
Testing procedure: A standardized procedure which requires choice of solvent for extraction. In PE determinations, xylene was used as a solvent.[119] A more complex procedure was used to determine the gel content in radiation crosslinked PVC filled with calcium carbonate.[120] The compound was extracted with tetrahydrofuran, and non-dissolved residue was determined. This residue was then used for determination of chlorine by the Schoniger method. From the amount of chlorine, the concentration of polymer was established. The remainder of the gel content was a filler embedded by gel.[120]
Standard methods: ASTM D 2765, ISO 19147
Major results: The total gel content in radiation crosslinked PVC was increased by the addition of calcium carbonate but only due to the inclusion of filler in gel. When filler content in gel was subtracted, the amount of polymer gel formed decreased as the addition of filler increased due to the stabilizing activity of the filler.[120]

14.2.6 INFRARED AND RAMAN SPECTROSCOPY[48,7985,89,94,106,109,121-138]

Applications: The following use was made of infrared and Raman spectroscopy: identification of surface groups on treated and untreated fumed silica,[109] identification of silica functional groups and coatings by Raman spectroscopy,[122] silane deposition on various fillers,[127] surface grafting of barium sulfate by acryloamide grafting of wood fiber,[106] spectral absorption of filler,[89,126] crystallization of polymer in the presence of filler,[79] absorption of polyacrylate on alumina,[121] deformation of fibers in composites by Raman spectroscopy,[123] the effect of fillers on UV cure,[124] the effect of zeolite on PVDF crystalline structure,[125] kaolin modification by PEG,[126] characterization of carbon fibers by Raman spectroscopy,[130] the effect of strain on the Raman spectrum of carbon fiber,[134] characterization of carbon fiber by IR,[135] interaction of filler with ZnO,[131] interaction of talc with LDPE,[132] formation of zinc carboxylates during UV irradiation of PE,[138] and photodegradation of polychloroprene in the presence of carbon black.[137]

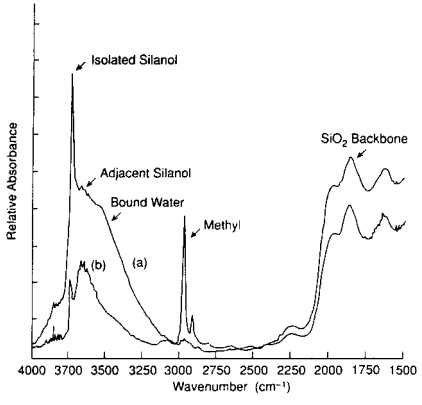

Figure 14.27. Infrared spectra of fumed silica. [Adapted, by permission, from Zumbrum M A, *J. Adhesion*, **46**, Nos.1-4, 1994, 181-96.]

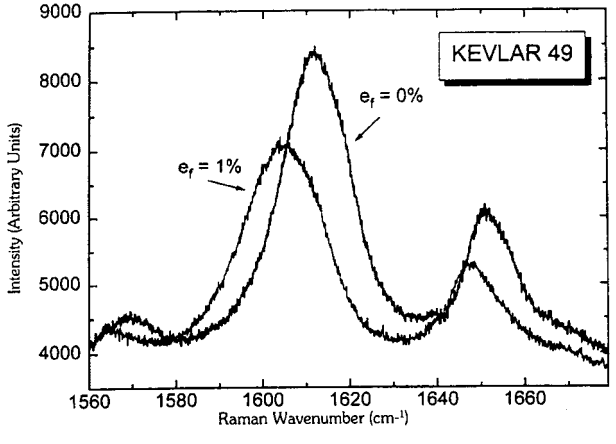

Figure 14.28. Strain induced shift of Raman spectra for a single filament Kevlar. [Adapted, by permission, from Young R J, *Prog. Rubb. Plast. Technol*., **11**, No.2, 1995, 124-36.]

Testing procedure: In general, standard methods were used, with some improvements to obtain better resolution. A photoacoustic detector was used to obtain spectra of fumed silica.[109] A carbon black background was used. In studies of adhesion of coatings on metal substrates, a gold coated background was used as the reference spectrum.[48] Diffuse reflectance spectra, DRIFT, were used to characterize surface species on alumina[121] and kaolin.[126] A Raman microprobe was capable of obtaining spectra from a very small area (2 μm

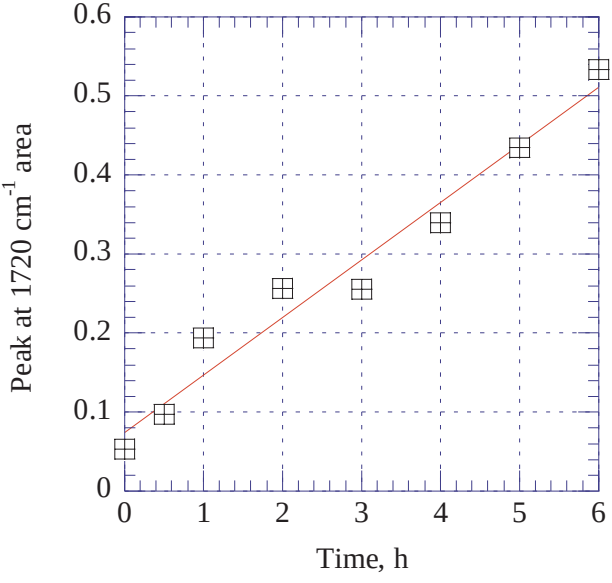

Figure 14.29. Peak surface areas at 1720 cm^{-1} vs. treatment time of carbon fibers. [Data from Ohwaki T, Ishida H, *J. Adhesion*, **52**, Nos.1-4, 1995, 167-86.]

in diameter).[123] A Raman frequency shift was used to study the effect of strain on carbon fiber.[134]

Standard methods: not applicable

Major results: Figure 14.27 compares the IR spectra of silane-treated and untreated silica. The major difference is in the concentration of functional groups, which are numerous in untreated silica and few in the treated version. Raman spectroscopy was found very useful in determination of functional groups on silica and other fillers.[122] Figure 14.28 demonstrates the effect of strain on the shift in a Raman band of Kevlar fiber.[123] Two main bands at 1610 and 1645 cm^{-1} shift significantly to a lower wavenumber on application of strain. Further studies revealed that there is a very good linear correlation between strain and the 1610 cm^{-1} band shift. Group assignment of kaolin and modified kaolin using diffuse reflectance IR was published.[126] Talc presence in a formulation can be easily recognized on an IR spectrum.[89,132] Oxidation of carbon fiber can be monitored by FTIR measurements (Figure 14.29). Two peaks on the IR spectrum (1720 and 1580 cm^{-1}) have a linear correlation with treatment time.[135]

14.2.7 NUCLEAR MAGNETIC RESONANCE SPECTROSCOPY[64,124,126,139-153]

Applications: NMR has found the following applications in filled systems: carbon black adsorption of SBR,[141] the effect of carbon black loading on cure rate of natural rubber,[148] gel-like behavior of polybutadiene/carbon black mixtures,[150] structure and dynamics of carbon black filled rubber vulcanizates,[153] interaction of

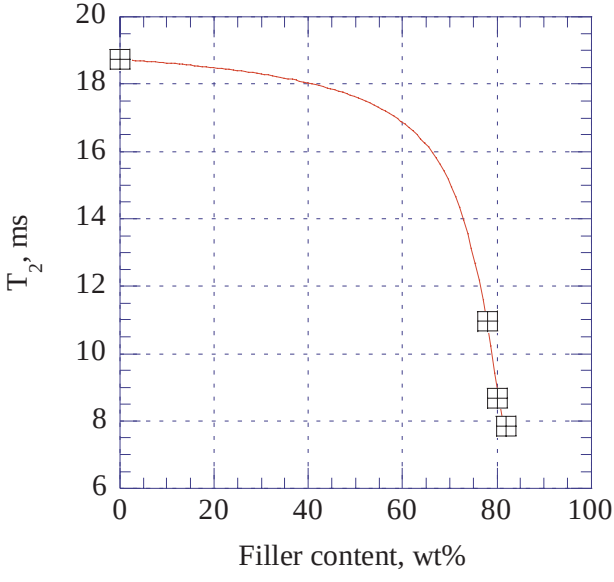

Figure 14.30 Relaxation time, T_2, vs. filler concentration in solid racket propellant. [Data from Merwin L H, Nissan R A, Stephens T S, Wallner A S, *J. Appl. Polym. Sci.*, **62**, No.2, 1996, 341-8.]

kaolin, $BaSO_4$, lithopone and ZnS with EPDM,[152] determination of the effect of filler on T_2 relaxation times and MRI imaging (see Section 14.1.16),[64] comparison of filled and unfilled UV-curable systems containing $Al(OH)_3$,[124] determination of chemical shifts on modified kaolin,[126] structure comparison of PMMA filled with $Al(OH)_3$,[139] curing of duroplasts in the presence of fillers,[140] structure and dynamics of PMMA/colloidal silica composite,[147] crystallization of PDMS in the presence of silica,[142] stress distribution in filled PDMS by NMR imaging,[143] interaction between silica and rubbers,[145] oxidative aging of carbon black-filled SBR by NMR imaging,[144] crosslink density of filled natural rubber,[146] the effect of carbon black on T_2,[146] characterization of absorbed water in aramid fiber,[149] and mobility of hydrocarbon chains in barium sulphate containing nanocomposite.[151] Numerous applications show the versatility of NMR applications in filled systems, which is due to the possibility of use of solid samples and evaluation of molecular mobility.

Testing procedure: Several variations of NMR were used as follows: MRI (magnetic resonance imaging),[64,144] solid-state ^{13}C NMR,[124,126,139,140,146,147,148,153] ^{1}H NMR,[141,143,146,149,152] ^{29}Si NMR,[147] ^{23}Na NMR,[149] magic angle,[141,146,147,148,149]

Standard methods: not applicable

Major results: Figure 14.30 shows the relationship between relaxation time, T_2, and amount of filler in solid racket propellant.[64] Relaxation time decreases with filler load because the material becomes more rigid with increasing filler loading. Urethane carbonyl, and aromatic carbons were found among others in kaolin modified by urethane.[126] Conformational changes in PMMA were found in a strongly inter-

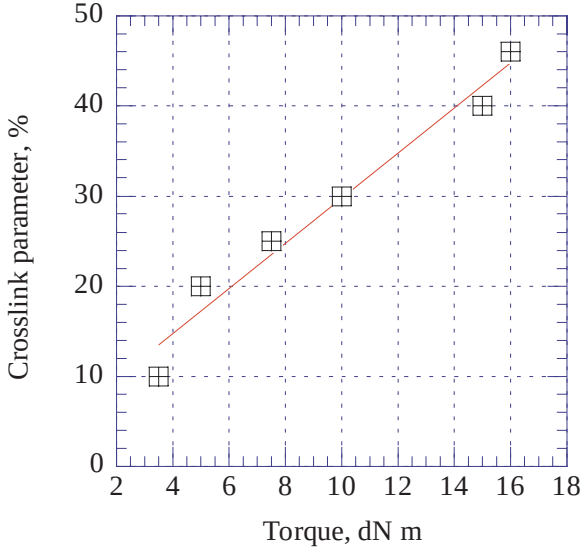

Figure 14.31. Crosslink parameter vs. torque for carbon black filled SBR. [Adapted, by permission, from Fuelber C, Bluemich B, Unseld K, Herrmann V, *Kaut. u. Gummi Kunst*., **48**, No.4, 1995, 254-9.]

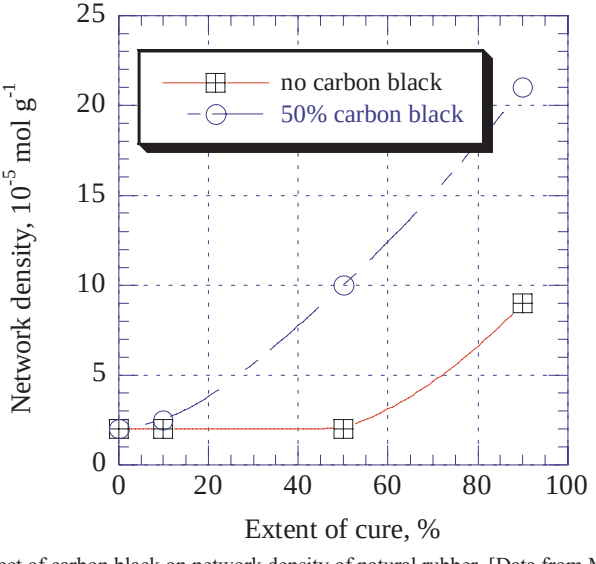

Figure 14.32. The effect of carbon black on network density of natural rubber. [Data from Mori M, Koenig J L, *Rubb. Chem. Technol.,* **68**, No.4, 1995, 551-62.]

acting system with alumina.[139] Figure 14.31 shows correlation of the NMR crosslink parameter, δ, with vulcameter torque.[144] This results are in agreement with theory and show the precision of measurement which can be attained. Figure 14.32 shows that carbon black increases the network density of vulcanized rubber.[148]

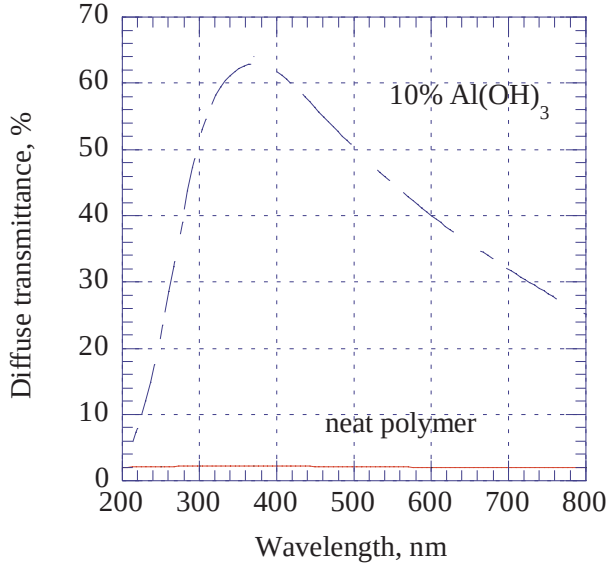

Figure 14.33. Relative diffuse UV/VIS transmittance spectra of PU after UV cure. [Data from Parker A A, Martin E S, Clever T R, *J. Coatings Technol*., **66**, No.829, 1994, 39-46.]

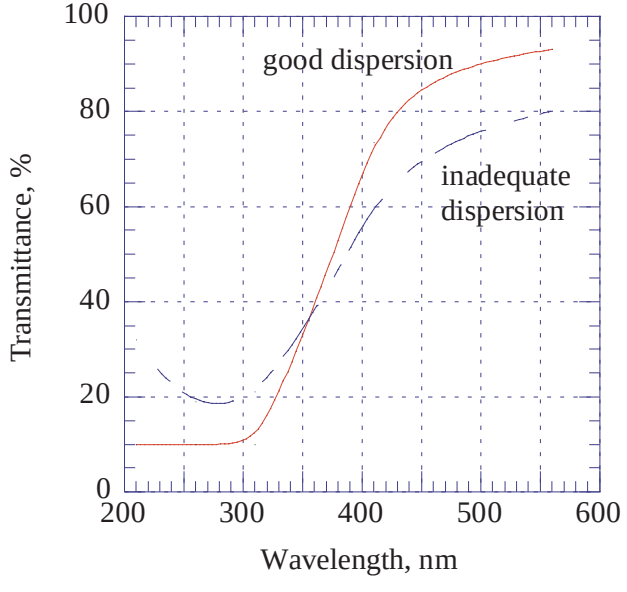

Figure 14.34. UV/VIS spectra of good and bad dispersions. [Data from Gaw F, Enhancing polymers using additives and modifiers, Symposium, Shawbury, 1993.]

14.2.8 UV AND VISIBLE SPECTROPHOTOMETRY[40,59,124,154,155]

Applications: Due to the nature of fillers, UV and visible spectroscopy is not the most popular method of testing, but there is some useful information which can be obtained from these methods. The following information can be found in the cur-

rent literature: the effect of fillers on UV cure of coatings,[124] UV spectrum of a nanocomposite,[59] determination of conjugated double bonds in PE, [40] the effect of dispersion on the UV-visible spectrum of TiO_2 filled materials,[154] the effect of crystal diameter on the relative opacity of TiO_2,[155] and the effect of ultrafine TiO_2 on the UV-visible spectrum of PP.[155]
Major results: Figure 14.33 shows relative diffuse UV/VIS transmittance spectra for PU films filled with $Al(OH)_3$. This finding corresponds with a higher rate of UV cure of system containing filler.[124] Poor dispersion of TiO_2 reduces absorption of UV and imparts whiteness due to the scattering of visible light (Figure 14.34).[154]

14.2.9 X-RAY ANALYSIS[55,59,85,89,98,103,156-165]

Applications: Numerous uses of x-ray analysis were reported for filled systems. They include: orientation of talc particles in extruded thermoplastics,[55,89,163,165] particle size determination in nanocomposites,[59] crystallinity of talc nucleated PP,[85] crystallinity of polymerization filled PE,[98] diffraction pattern of filled PVA,[103] structure of nanocomposites based on montmorillonite,[156] degree of filler mixing,[157] structural characteristics of fillers,[158,159] structure of carbon black filled rubber,[160] the effect of apatite concentration on the structure of wood pulp,[161] and graphite as template.[164] This list shows the versatility of the method in applications to filled systems.
Testing procedure: The testing procedures are adjusted to the experiment, but in the majority of cases typical WAXS measurements are used.
Standard methods: not applicable
Major results: The results support other studies which is why no examples are given for this method.

14.2.10 X-RAY PHOTOELECTRON SPECTROSCOPY[12,59,102,128,135,166-174]

Applications: XPS was used for the following purposes: determination of elemental composition of nanocomposites,[59] the effect of oxidation and reduction of carbon fibers by monitoring the O/C ratio,[12,135,174] concentration of functional groups on the surface of carbon fibers,[12,166,174] elemental composition of the surface of carbon fibers,[166,168,171] the effect of surface coating on the surface composition of carbon fiber,[171] chemical degradation of carbon fibers,[171,172] fiber/matrix interface of sized carbon fiber,[173] the effect of fiber sizing technology on surface composition of carbon fibers,[173] surface analysis of barium sulfate modified by 12-hydroxystearate,[128] X-ray radiography of nickel-coated fibers,[167] surface atoms of hydroxyapatite,[169] coating analysis of silane treated hydroxyapatite,[169] and composition of the failure area of an adhesive joint between rubber and metal.[170] This review of applications shows that carbon fibers are the most frequently tested material by XPS.
Testing procedure: The methods of testing used were fairly standard techniques of equipment operation. It was mentioned[169] that the sampling depth of XPS (~50-100 Å) is sensitive enough to detect silane having a thickness of 5-10 monolayers.
Standard methods: ASTM E 902 (instrument calibration).

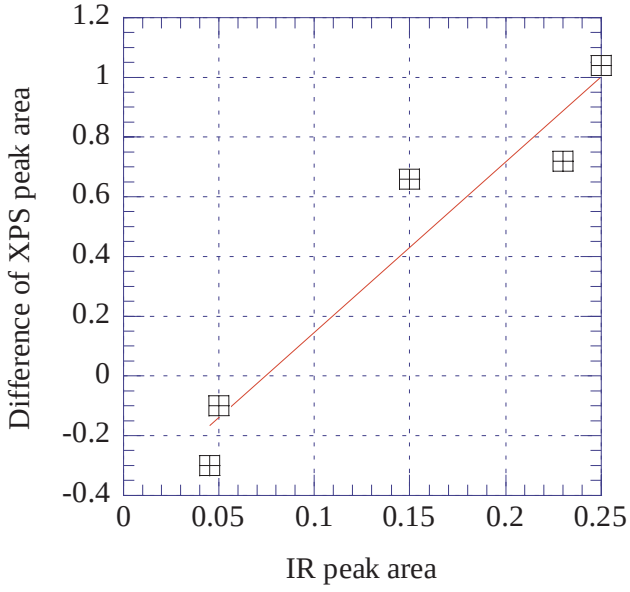

Figure 14.35. Plot of IR peak area vs. difference in XPS area. [Adapted, by permission, from Ohwaki T, Ishida H, *J. Adhesion*, **52**, Nos.1-4, 1995, 167-86.]

Major results: Figure 14.35 shows the correlation between IR peak area and difference of XPS peak area.[135] The IR peak area is at 1720 cm^{-1}, and the XPS peak area difference is at 288.4 eV. Both peaks were assigned to C=O. The results obtained by the two methods show a good correlation. Figure 6.7 shows the effect of treatment time by oxygen plasma of carbon fiber on the O/C elemental ratio vs. treatment time. A plateau is reached after a short period of treatment.

REFERENCES

1 Wawkuschewski A, Cantow H J, Magonov S N, *Polym. Bull*., **32**, No.2, 1994, 235-40.
2 Srinivasan G, Reneker D H, *Polym. Int*., **36**, No.2, 1995, 195-201.
3 Donnet J B, Custodero E, Wang T K, *Kaut. u. Gummi Kunst*., **49**, No.4, 1996, 274-9.
4 Costa L, Camino G, Bertelli G, Borsini G, *Fire & Mat*., **19**, No.3, 1995, 133-42.
5 Karasek L, Sumita M, *J. Mat. Sci.*, **31**, No.2, 1996, 281-9.
6 Levesque J L, Fraval J T, Antec '93. Conference Proceedings, New Orleans, La., 9th-13th May 1993, Vol. II, 1957-64.
7 Hirschler M, Flame Retardants '96. Conference proceedings, London, 17th-18th Jan.1996, 199-214.
8 Cusack P, Flame Retardants '96. Conference proceedings, London, 17th-18th Jan.1996, 57-69.
9 Ferm D J, Shen K K, Antec '94. Conference Proceedings, San Francisco, Ca., 1st-5th May 1994, Vol.III, 3522-6.
10 Whiteley R H, Elliot P J, Staggs J E, Flame Retardants '96. Conference proceedings, London, 17th-18th Jan.1996, 70-8.
11 Pape P G, Romenesko D J, Antec '97. Conference proceedings, Toronto, April 1997, 2941-52.
12 Tang L-G, Kardos J L, *Polym. Composites*, **18**, No.1, 1997, 100-13.
13 Balard H, Papirer E, *Prog. Org. Coatings*, **22**, No.1-4, 1993, 1-17.
14 Godard P, Bomal Y, Biebuyck J J, *J. Mat. Sci*., **28**, No.24, 1993, 6605-10.
15 Hegedus C R, Kamel I L, J. *Coatings Technol*., **65**, No.820, 1993, 23-30.
16 Molphy M, Mainwaring D E, Rizzardo E, Gunatillake P A, Laslett R L, *Polym. Int*., **37**, No.1,

1995, 53-61.
17 OgawaT, Ikeda M, *J. Adhesion,* **43**, Nos.1-2, 1993, 69-78.
18 Donnet J B, Wang W, Vidal A, Wang M J, *Kaut. u. Gummi Kunst*., **4**6, No.11, Nov.1993, 866-71.
19 Wang W D, Haidar B, Vidal A, Donnet J B, *Kaut. u. Gummi Kunst*., **47**, No.4, 1994, 238-41.
20 Zaborskaya L V, Dovgualo V A, Yurkevich O R, *J. Adhesion Sci. Technol*., **9**, No.1, 1995, 61-71.
21 Al-Turaif H, Unertl W N, Lepoutre P, *J. Adhesion Sci. Technol*., **9**, No.7, 1995, 801-11.
22 Lee I, *J. Mat. Sci*., **30**, No.23, 1995, 6019-22.
23 Bomal Y, Godard P, *Polym. Engng. Sci*., **36**, No.2, 1996, 237-43.
24 Gatenhom P, Hedenberg P, Karlsson J, Felix J, Antec '96. Volume II. Conference proceedings, Indianapolis, 5th-10th May 1996, 2302-4.
25 Torro-Palau A, Fernandez-Garcia J C, Orgiles-Barcelo A C, Martin-Martinez J M, *J. Adhesion*, **57**, Nos.1-4, 1996, 203-25.
26 Foster J K, Sims E S, Venable S W, *Paint & Ink Int*., **8**, No.3, 1995, 18-21.
27 Hollis R D, Hyche K W, Color and Appearance Retec: Effects in Plastics. Conference proceedings, Oak Brook, Il., 20th-22nd Sept.1994, 94-105.
28 Scott D M, *Composites, Part A*, **28A**, 1997, 703-7.
29 Yazici R, Kalyon D M, Antec '93. Conference Proceedings, New Orleans, La., 9th-13th May 1993, Vol. III, 2845-50.
30 Guerbe L, Freakley P K, *Kaut. u. Gummi Kunst*., **48**, No.4, 1995, 260-9.
31 Toure B, Lopez-Cuesta J, Benhassaine A, Crespy A, *Int. J. Polym. Analysis and Characterization*, **2**, No.3, 1996, 193-202.
32 Frounchi M, Burford R P, Chaplin R P, *Polym. & Polym. Composites*, **2**, No.2, 1994, 77-82.
33 Dole P, Chauchard J, *Polym. Degradat. Stabil*., **47**, No.3, 1995, 441-8.
34 Brovkop O O, Sergeeva L M, Slinchenko O A, Fainleib O M, *Polym. Int*., **40**, No.4, 1996, 299-305.
35 Lei Yang, Schruben D L, *Polym. Engng. Sci*., **34**, No.14, 1994, 1109-14.
36 Mamunya E P, Davidenko V V, Lebedev E V, *Polym. Composites*, **16**, No.4, 1995, 319-24.
37 Gokturk H S, Fiske T J, Kalyon D M, Antec '93. Conference Proceedings, New Orleans, La., 9th-13th May 1993, Vol. I, 605-8.
38 Van Beek G A, Pang S S, Lea R H, Antec '93. Conference Proceedings, New Orleans, La., 9th-13th May 1993, Vol. I, 602-4.
39 Nasr G M, Badawy M M, Gwaily S E, Shash N M, Hassan H H, *Polym. Degradat. Stabil.,* **48**, No.2, 1995, 237-41.
40 Svorcik V, Micek I, Jankovskij O, Rybka V, Hnatowicz V, Wang L, Angert N, *Polym. Degradat. Stabil*., **55**, 1997, 115-21.
41 Wu S-L, Tung I-C, *Polym. Composites*, **16**, No.3, 1995, 233-9.
42 Saad A L G, Younan A F, *Polym. Degradat. Stabil*., **50**, No.2, 1995, 133-40.
43 Meng-Jiao Wang, Wolff S, Freund B, *Rubb. Chem. Technol*., **67**, No.1, 1994, 27-41.
44 Zihlif A M, Di Liello V, Martuscelli E, Ragosta G, *Int. J. Polym. Mat*., **29**, Nos.3-4, 1995, 211-20.
45 Maas S, Gronski W, *Kaut. u. Gummi Kunst*., **47**, No.6, 1994, 409-15.
46 Topoleski L D T, Ducheyne P, Cuckler J M, *J. Biomed. Mat. Res*., **29**, No.3, 1995, 299-307.
47 Tamura J, Kawanabe K, Yamamuro T, Nakamura T, Kokubo T, Yoshihara S, Shibuya T, *J. Biomed. Mat. Res*., **29**, No.5, 1995, 551-9.
48 Roche A A, Dole P, Bouzziri M, *J. Adhesion Sci. Technol*., **8**, No.6, 1994, 587-609.
49 Furtado C R G, Nunes R C R, de Siqueira Filho A S, *Polym. Bull*., **34**, No.5/6, 1995, 627-33.
50 Minkova L, Magagnini P L, *Polym. Degradat. Stabil*., **42**, No.1, 1993, 107-15.
51 Alkan C, Arslan M, Cici M, Kaya M, Aksoy M, *Resources Conserv. & Recycling*, **13**, Nos.3-4, 1995, 147-54.
52 Helbert W, Cavaille J Y, Dufresne A, *Polym. Composites*, **17**, No.4, 1996, 604-11.
53 Tchoudakov R, Breuer O, Narkis M, Siegmann A, *Polym. Engng. Sci*., **36**, No.10, 1996, 1336-46.
54 Casenave S, Ait-Kadi A, Brahimi B, Riedl B, Antec '95. Vol. II. Conference Proceedings, Boston, Ma., 7th-11th May 1995, 1438-42.
55 Kim K J, White J L, *J. of Non-Newtonian Fluid Mechanics*, **66**, Nos.2/3, 1996, 257-70.
56 Niedermeier W, Raab H, Maier P, Kreitmeier S, Goeritz D, *Kaut. u. Gummi Kunst*., **48**, No.9, 1995, 611-6.
57 Eisenbach C D, Ribbe A, Goeldel A, *Kaut. u. Gummi Kunst.*, **49**, No.6, 1996, 406-10.
58 Zhao W, Hasegawa S, Fujita J, Yoshii F, Sasaki T, Makuuchi K, Sun J, Nishimoto S, *Polym. Degradat. Stabil*., **53**, No.2, 1996, 199-206.
59 Jinman Huang, Yi Yang, Bai Yang, Shiyong Liu, Jiacong Shen, *Polym. Bull*., **37**, No.5, 1996, 679-82.

60 Wagner A H, Kalyon D M, Yazici R, Fiske T J, Antec '97. Conference proceedings, Toronto, April 1997, 996-1000.
61 Gerard P, Raine J, Pabiot J, Antec '97. Conference proceedings, Toronto, April 1997, 526-31.
62 Bay R S, Tucker C L, PhD thesis, University of Illinois, Urbana, 1991.
63 Hshieh F Y, Beson H D, *Fire Mater*., **21**, 1997, 41-9.
64 Merwin L H, Nissan R A, Stephens T S, Wallner A S, *J. Appl. Polym. Sci.*, **62**, No.2, 1996, 341-8.
65 Haynes A R, Coates P D, *J. Mat. Sci.*, **31**, No.7, 1996, 1843-55.
66 Kody R S, Martin D C, *Polym. Engng. Sci*., **36**, No.2, 1996, 298-304.
67 Averous L, Quantin J C, Lafon D, Crespy A, *Int. J. Polym. Analysis and Characterization*, **1**, No.4, 1995, 339-47.
68 Herzig R, Baker W E, *J. Mat. Sci*., **28**, No.24, 1993, 6531-9.
69 Benrashid R, Nelson G L, *J. Fire Sci*., **11**, No.5, 1993, 371-93.
70 Fiske T J, Gokturk H S, Kalyon D M, Antec '93. Conference Proceedings, New Orleans, La., 9th-13th May 1993, Vol. I, 614-7.
71 Godovsky D Yu, *Adv. Polym. Sci*., **119**, 1995, 81-122.
72 Herd C R, Meeting of the Rubber Division, ACS, Montreal, May 5-8, 1996, paper B.
73 Gerspacher M, O'Farrell C P, Yang H H, Wampler W A, Meeting of the Rubber Division, ACS, Montreal, May 5-8, 1996, paper C.
74 Lisy F, Hiltner A, Baer E, Katz J L, Meunier A, *J. Appl. Polym. Sci.*, **52**, No.2, 1994, 329-52.
75 Ohta M, Nakamura Y, Hamada H, Maekawa Z, *Polym. & Polym. Composites*, **2**, No.4, 1994, 215-21.
76 Nguyen T N, Lethiecq M, Levassort F, Patat F, *Int. J. Polym. Analysis and Characterization*, **1**, No.4, 1995, 277-87.
77 Gendron R, Daigneault L E, Tatibouet J, Dumoulin M M, Antec '94. Conference Proceedings, San Francisco, Ca., 1st-5th May 1994, Vol. I, 167-71.
78 Maeda S, Armes S P, *Synthetic Metals*, **73**, No.2, 1995, 151-5.
79 Quintanilla L, Pastor J M, *Polymer*, **35**, No.24, 1994, 5241-6.
80 Peng W, Riedl B, *Polymer*, **35**, No.6, 1994, 1280-6.
81 del Rio C, Acosta J L, *Polymer*, **35**, No.17, 1994, 3752-7.
82 Modesti M, Simioni F, Albertin P, *Cell. Polym*., **13**, No.2, 1994, 113-24.
83 Privalko V P, Novikov V V, *Adv. Polym. Sci*., **119**, 1995, 31-77.
84 Bigg D M, **Thermal and Electrical Conductivity of Polymers Materials**, Eds. Godovsky Y K, Privalko V P, *Springer*, Berlin 1995.
85 Rabello M S, White J R, Antec '97. Conference proceedings, Toronto, April 1997, 2991-5.
86 Albertsson A-C, Barenstedt C, Karlsson S, *J. Environmental Polym. Degradat*., **1**, No.4, 1993, 241-5.
87 McNeill I C, Mohammed M H, *Polym. Degradat. Stabil*., **48**, No.1, 1995, 189-95.
88 Hajji P, Cavaille J Y, Favier V, Gauthier C, Vigier G, *Polym. Composites*, **17**, No.4, 1996, 612-9.
89 Rabello M S, White J R, *Polym. Composites*, **17**, No.5, 1996, 691-704.
90 Jang J, Yi J, *Polym. Engng. Sci*., **35**, No.20, 1995, 1583-91.
91 Kenny J M, Opalicki M, *Composites Part A: Applied Science and Manufacturing*, **27A**, No.3, 1996, 229-40.
92 McNeill I C, Mohammed M H, *Polym. Degradat. Stabil*., **49**, No.2, 1995, 263-73.
93 Schreiber H P, Antec '95. Vol. II. Conference Proceedings, Boston, Ma., 7th-11th May 1995, 2446-51.
94 Hornsby P R, Wang J, Rothon R, Jackson G, Wilkinson G, Cossick K, *Polym. Degradat. Stabil*., **51**, No.3, 1996, 235-49.
95 Toure B, Lopez Cuesta J M, Gaudon P, Benhassaine A, Crespy A, *Polym. Degradat. Stabil*., **53**, No.3, 1996, 371-9.
96 Toure B, Lopez Cuesta J-M, Longerey M, Crespy A, *Polym. Degradat. Stabil*., **54**, Nos 2-3, 1996, 345-52.
97 Sergeeva L M, Slinchenko E A, Brovko A A, Fainleib A M, Nedashkovskaya N S, *Polym. Sci., Ser. B*, **38**, Nos.5/6, 1996, 225-30.
98 Beloshenko V A, Kozlov G V, Slobodina V G, Prut E V, Grinev V G, *Polym. Sci., Ser. B*, **37**, Nos.5-6, 1995, 316-8.
99 Pukanszky B, Belina K, Rockenbauer A, Maurer F H J, *Composites*, **25**, No.3, 1994, 205-14.
100 Szocs F, Klimova M, Chodak I, Chorvath I, *Eur. Polym. J.*, **32**, No.3, 1996, 401-2.
101 Rockenbauer A, Korecz L, Pukanszky B, *Polym. Bull*., **33**, No.5, 1994, 585-9.
102 Chen L, Liu K, Yang C Z, *Polym. Bull.*, **37**, No.3, 1996, 377-83.
103 Suzuki F, Nakane K, Piao J-S, *J. Mat. Sci*., **31**, No.5, 1996, 1335-40.
104 Darmstadt H, Roy C, Kaliaguine S, Sahouli B, Blacher S, Pirard R, Brouers F, *Rubb. Chem. Technol*.,

68, No.2, 1995, 330-41.
105 Wang W, Vidal A, Donnet J-B, Wang M-J, *Kaut. u. Gummi Kunst.*, **46**, No.12, Dec.1993, 933-40.
106 Sain M M, Kokta B V, Antec '93. Conference Proceedings, New Orleans, La., 9th-13th May 1993, Vol. I, 320-4.
107 Garbow J R, Asrar J, Hardiman C J, *Chem. of Mat.*, **5**, No.6, 1993, 869-75.
108 Hegedus C R, Kamel I L, *J. Coatings Technol.*, **65**, No.820, 1993, 31-43
109 Zumbrum M A, *J. Adhesion*, **46**, Nos.1-4, 1994, 181-96.
110 Vidal A, Wang W, Donnet J B, *Kaut. u. Gummi Kunst.*, **46**, No.10, 1993, 770-8.
111 Donnet J B, *Kaut. u. Gummi Kunst.*, **47**, No.9, 1994, 628-32.
112 Zaborski M, Slusarski L, Donnet J B, Papirer E, *Kaut. u. Gummi Kunst.*, **47**, No.10, 1994, 730-8.
113 Ulkem I, Bataille P, Schreiber H P, *J. Macromol. Sci. A*, **31**, No.3, 1994, 291-303.
114 Rebouillat S, Escoubes M, Gauthier R, Vigier A, *J. Appl. Polym. Sci.*, **5**8, No.8, 1995, 1305-15.
115 Balard H, Saada A, Hartmann J, Aouadj O, Papirer E, *Macromol. Symp.*, **108**, 1996, 63-80.
116 Persson A L, Bertilsson H, *Composite Interfaces*, **3**, No.4, 1996, 321-32.
117 Kettrup A A, Lenoir D, Thumm W, Kampke-Thiel K, Beck B, *Polym. Degradat. Stabil.*, **54**, Nos 2-3, 1996, 175-80.
118 Ryabikova V M, Zigel A N, Sverdlova S I, Vinogradova G A, *Int. Polym. Sci. Technol.*, **23**, No.1, 1996, T/89-90.
119 Yeh J T, Yang H M, Huang S S, *Polym. Degradat. Stabil.*, **50**, No.2, 1995, 229-34.
120 Chudinova V V, Guzeev V V, Mozzhukhin V B, Pomerantseva E G, Nozrina F D, Zhil'tsov V V, Zubov V P, *Int. Polym. Sci. Technol.,* **21**, No.10, 1994, T/102-4.
121 Lee D H, Condrate R A, Reed J S, *J. Mater. Sci.*, **32**, 1997, 471-8.
122 Gailliez-Degremont E, Bacquet M, Laureyns J, Morcellet M, *J. Appl. Polym. Sci.*, **65**, 1997, 871-82.
123 Young R J, *Prog. Rubb. Plast. Technol.*, **11**, No.2, 1995, 124-36.
124 Parker A A, Martin E S, Clever T R, *J. Coatings Technol.*, **66**, No.829, 1994, 39-46.
125 Abramova N A, Diikova E U, Lyakhovskii Yu Z, *Polym. Sci.*, **36**, No.9, 1994, 1308-9.
126 Molphy M, Laslett R L, Gunatillake P A, Rizzardo E, Mainwaring D E, *Polym. Int.*, **34**, No.4, 1994, 425-31.
127 Zolotnitsky M, Steinmetz J R, *J. Vinyl and Additive Technol.*, **1**, No.2, 1995, 109-13.
128 Tsubokawa N, Seno K, *J. Macromol. Sci. A*, **31**, No.9, 1994, 1135-45.
129 Gerspacher M, O'Farrel C P, Wampler W A, *Rubb. World*, **212**, No.3, 1995, 26-9.
130 Melanitis N, Tetlow P L, Galiotis C, *J. Mat. Sci.*, **31**, No.4, 1996, 851-60.
131 Datta S, Bhattacharya A K, De S K, Kontos E G, Wefer J M, *Polymer*, **37**, No.12, 1996, 2581-5.
132 Singhal A, Fina L J, *Polymer*, **37**, No.12, 1996, 2335-43.
133 Caillaud J L, Deguillaume S, Vincent M, Giannotta J C, Widmaier J M, *Polym. Int.*, **40**, No.1, 1996, 1-7.
134 Leveque D, Auvray M H, *Composites Sci. & Technol.*, **56**, No.7, 1996, 749-54.
135 Ohwaki T, Ishida H, *J. Adhesion*, **52**, Nos.1-4, 1995, 167-86.
136 Sanchez-Solis A, Estrada M R, *Polym. Degradat. Stabil.*, **52**, No.3, 1996, 305-9.
137 Delor F, Lacoste J, Lemaire J, Barrois-Oudin N, Cardinet C, *Polym. Degradat. Stabil.*, **53**, No.3, 1996, 361-9.
138 Gordienko V P, Dmitriev Y A, *Polym. Sci., Ser. B*, **37**, Nos.5-6, 1995, 249-50.
139 Grohens Y, Schultz J, *Int. J. Adhesion Adhesives*, **17**, 1997, 163-7.
140 Domke W D, Halmheu F, Schneider S, *J. Appl. Polym. Sci.*, **54**, No.1, 1994, 83-90.
141 Dutta N K, Choudhury N R, Haidar B, Vidal A, Donnet J B, Delmotte L, Chezeau J M, *Polymer*, **35**, No.20, 1994, 4293-9.
142 Ebengou R H, Cohen-Addad J P, *Polymer*, **35**, No.14, 1994, 2962-9.
143 Bluemler P, Bluemich B, *Acta Polymerica*, **44**, No.3, 1993, 125-31.
144 Fuelber C, Bluemich B, Unseld K, Herrmann V, *Kaut. u. Gummi Kunst.*, **48**, No.4, 1995, 254-9.
145 Ou Y C, Yu Z Z, Vidal A, Donnet J B, *J. Appl. Polym. Sci.*, **59**, No.8, 1996, 1321-8.
146 Legrand A P, *Macromol. Symp.*, **108**, 1996, 81-96.
147 Joseph R, Zhang S, Ford W T, *Macromolecules*, **29**, No.4, 1996, 1305-12.
148 Mori M, Koenig J L, *Rubb. Chem. Technol.,* **68**, No.4, 1995, 551-62.
149 Connor C, Chadwick M M, *J. Mat. Sci.,* **31**, No.14, 1996, 3871-7.
150 Addad J P C, Frebourg P, *Polymer*, **37**, No.19, 1996, 4235-42.
151 Erofeev L N, Raevskii A V, Pisarenko T I, Grishin B S, *Int. Polym. Sci. Technol.*, **23**, No.5, 1996, T/12-4.
152 Hess M, Veeman W, Magusin P, Antec '96. Volume III. Conference proceedings, Indianapolis,

5th-10th May 1996, p.3682-6.
153 Heuert U, Knorgen M, Menge H, Scheler G, Schneider H, *Polym.Bull.*, **37**, No.4, Oct.1996, 489-96.
154 Gaw F M, Enhancing Polymers Using Additives and Modifiers, Rapra, Shawbury, 1993.
155 Robertson D R, Gaw F, AddCon '95, Basel, 1995.
156 Wu J, Lerner M M, *Chem. of Mat.*, **5**, No.6, 1993, 835-8.
157 Yazici R, Kalyon D M, Antec '97. Conference proceedings, Toronto, April 1997, 2076-80.
158 Kovacevic V, Lucic S, Hace D, Glasnovic A, Smit I, Bravar M, *J. Adhesion*, **47**, No.1-3, 1994, 201-15.
159 Anantharaman M R, Kurian P, Banerjee B, Mohamed E M, George M, *Kaut. u. Gummi Kunst.*, **49**, No.6, 1996, 424-6.
160 Strauss M, Pieper T, Peng W, Kilian H G, *Makromol. Chem., Macromol. Symp*., **76**, 1993, 131-6.
161 Nagieb Z A, El-Sakr N S, *Polym. Degradat. Stabil*., **57**, 1997, 205-9.
162 Le Bras M, Bourbigot, Le Tallec Y, Laureyns J., *Polym. Degradat. Stabil*., **56**, 1997, 11-21.
163 Suh C H, White J L, *Polym. Engng. Sci*., **36**, No.17, 1996 2188-97.
164 Isayama M, Nomiyama K, Kunitake T, *Adv. Mat*., **8**, No.8, 1996, 641-4.
165 Suh C H, White J L, Antec '96. Vol.I. Conference Proceedings, Indianapolis, 5th-10th May 1996, p.958-62.
166 Wang P H, Hong K L, Zhu Q R, *J. Appl. Polym. Sci*., **62**, No.12, 1996, 1987-91.
167 Guanghong Lu, Xiaotian Li, Hancheng Jiang, *Composites Sci. & Technol*., **56**, No.2, 1996, 193-200.
168 Tsutsumi K, Ban K, Shibata K, Okazaki S, Kogoma M, *J. Adhesion*, **57**, Nos.1-4, 1996, 45-53.
169 Dupraz A M P, de Wijn J R, v. d. Meer S A T, de Groot K, *J. Biomed. Mat. Res*., **30**, No.2, 1996, 231-8.
170 Jacks J, *Plast. Rubb.* Tiejun Wang, Sherwood P M A, *Chem. of Mat*., **7**, No.5, 1995, 1031-40. Wkly., No.1667, 1996, 7.
171 Tiejun Wang, Sherwood P M A, *Chem. of Mat*., **7**, No.5, 1995, 1031-40.
172 Wang T, Sherwood P M A, *Chem. of Mat*., **6**, No.6, 1994, 788-95.
173 Reis M J, Do Rego A M B, Da Silva J D L, *J. Mat. Sci*., **30**, No.1, 1995, 118-26.
174 Byung Suk Jin, Kwang Hee Lee, Chul Rim Choe, *Polym. Int*., **34**, No.2, 1994, 181-5.